Particles and the Cosmos

2019/2020

Sascha Caron, Jörg Hörandel

NM109
first semester, 6 ec

32 hrs lecture Wednesday 10:30 - 12:15 HG 00.086
32 hrs problem session Thursday 13:30 - 15:15 HG 02.052

Lectures:

Experimental methods (JRH)
04.09.2019 1. Interactions with matter
11.09.2019 2. Detectors
Standard model (SC)
18.09.2019 3. Particles, QED, Feynman rules
25.09.2019 4. Hadrons and QCD
02.10.2019 5. Hadrons and QCD
09.10.2019 6. Weak interactions, CP violation
16.10.2019 7. Higgs mechanism
Astroparticle physics (JRH)
06.11.2019 8. The birth of cosmic rays
13.11.2019 9. Cosmic rays in the Galaxy, in the heliosphere, and the Earth magnetic field
20.11.2019 10. Cosmic rays at the top of and in the atmosphere
27.11.2019 11. Cosmic rays underground - neutrino oscillations
04.12.2019 12. Neutrino oscillations, Astroparticle Physics
Beyond the Standard Model, Dark Matter (SC)
11.12.2019 13. Lambda CDM, Big-bang nucleosynthesis
18.12.2019 14. Dark matter - Beyond-the-standard-model reasons

for Astroparticle Physics

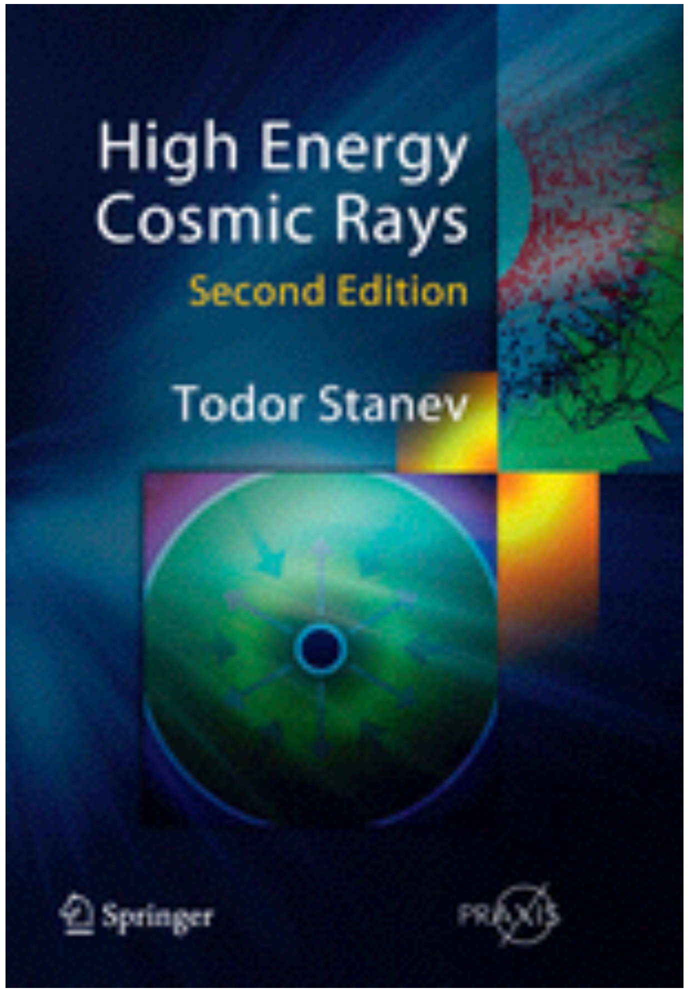

Jörg R. Hörandel
HG 02.721
http://particle.astro.ru.nl

Rafael Alves Batista
email: r.batista@astro.ru.nl


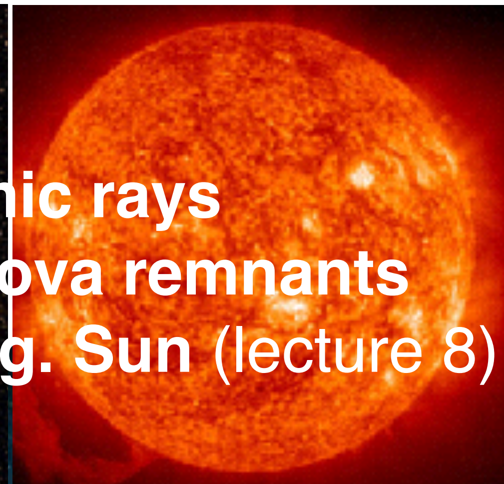

birth of cosmic rays
CRs: supernova remnants
neutrinos: e.g. Sun (lecture 8)

propagation of CRs in the Galaxy
interactions with ISM (lecture 9)

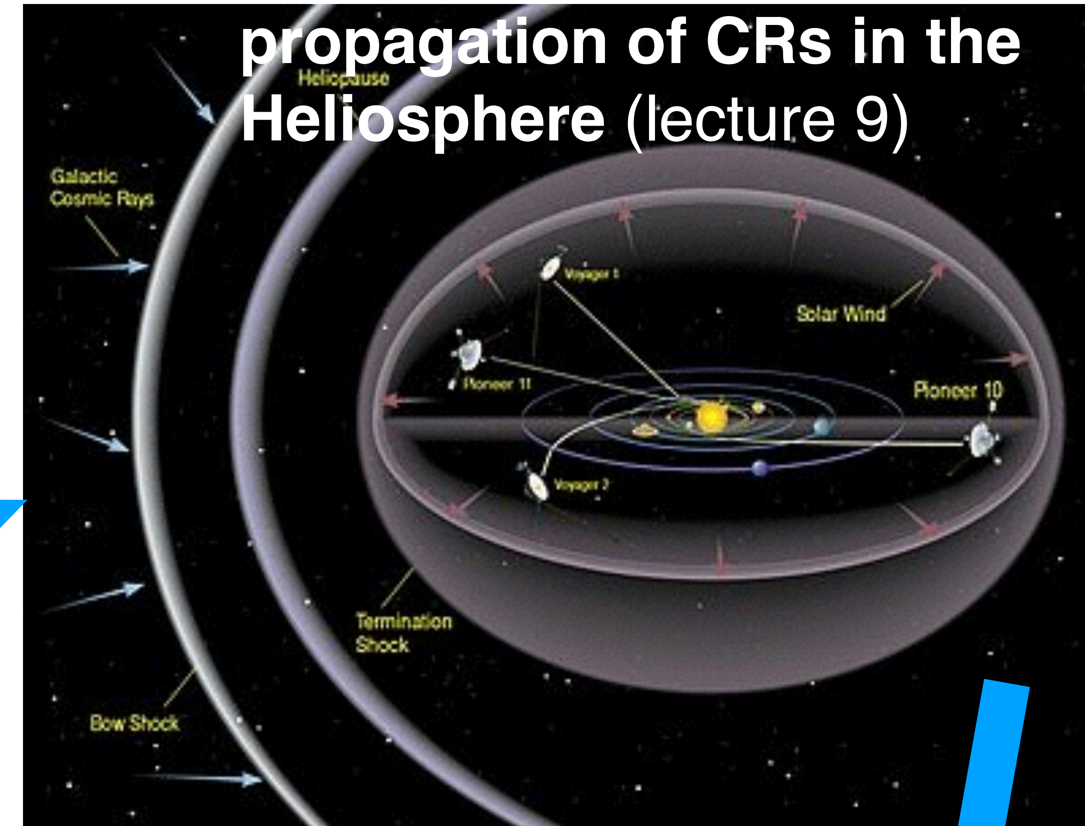

propagation of CRs in the Heliosphere (lecture 9)

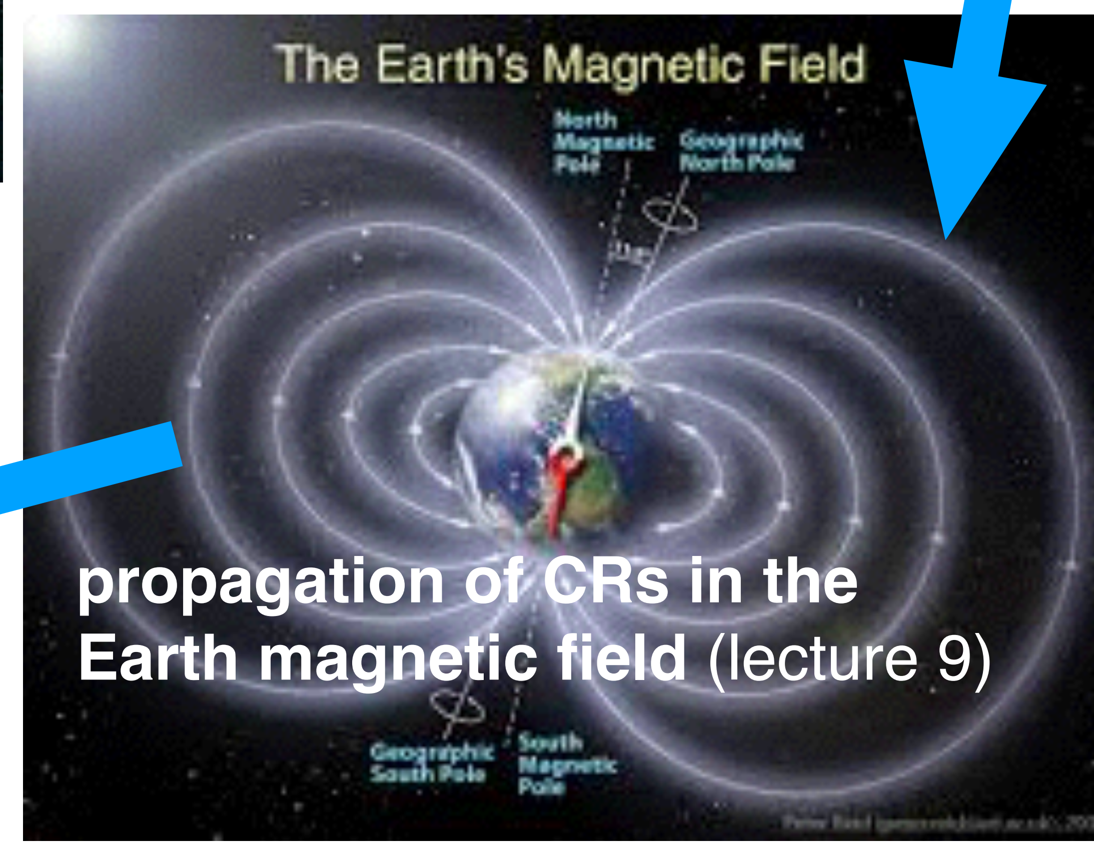

propagation of CRs in the Earth magnetic field (lecture 9)

CRs at the top of the atmosphere (lecture 10)

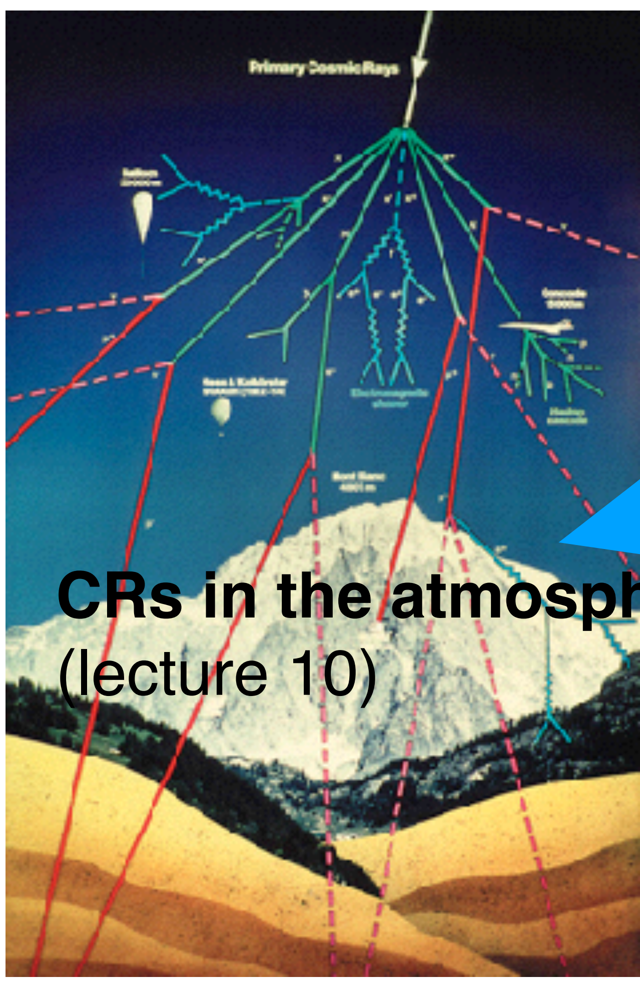

CRs in the atmosphere (lecture 10)

CRs underground (lecture 11)
neutrino oscillations (lecture 11+12)

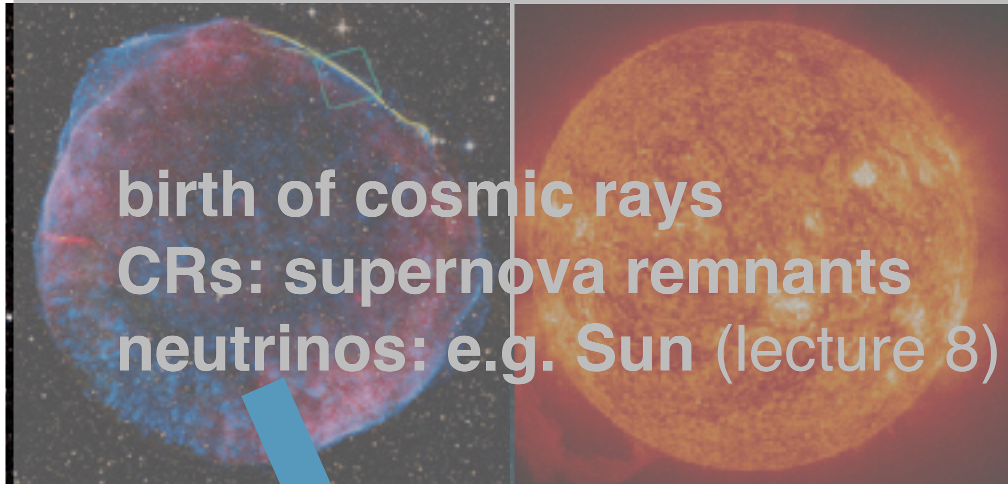

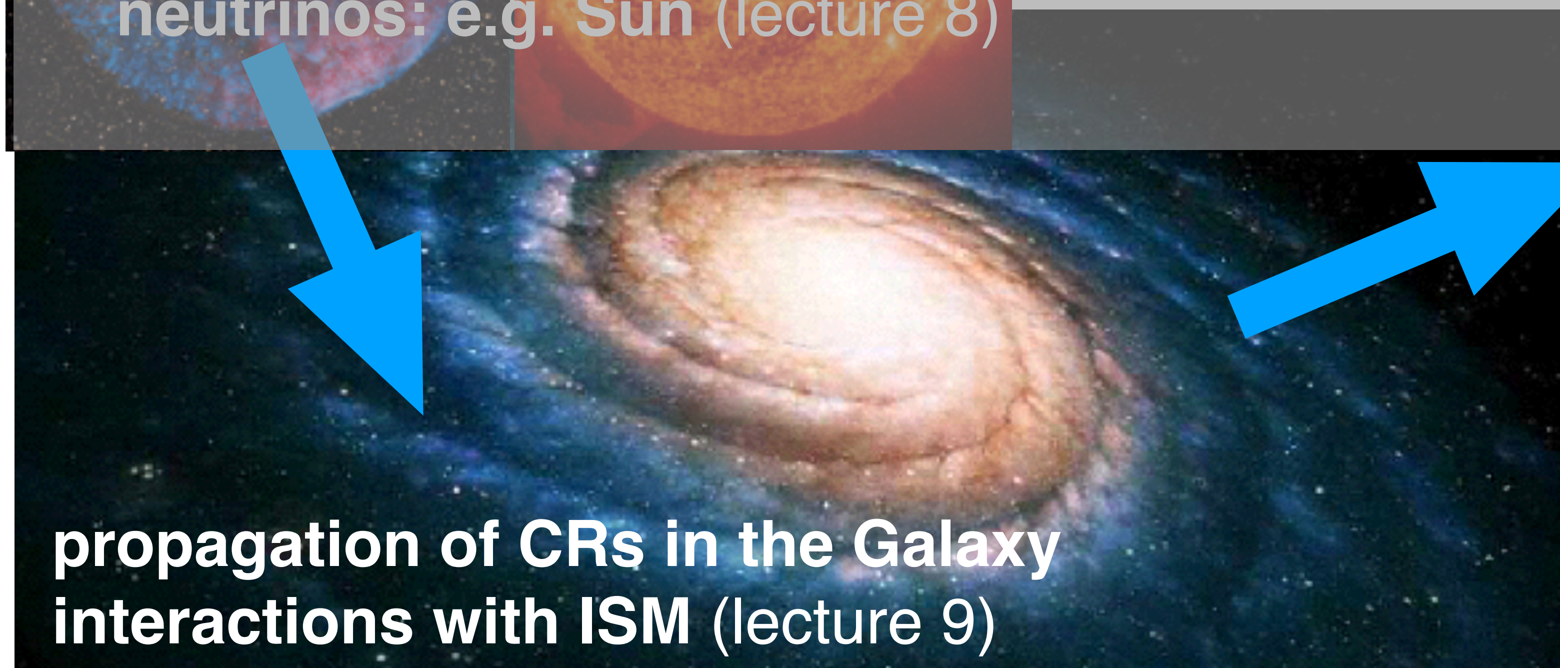

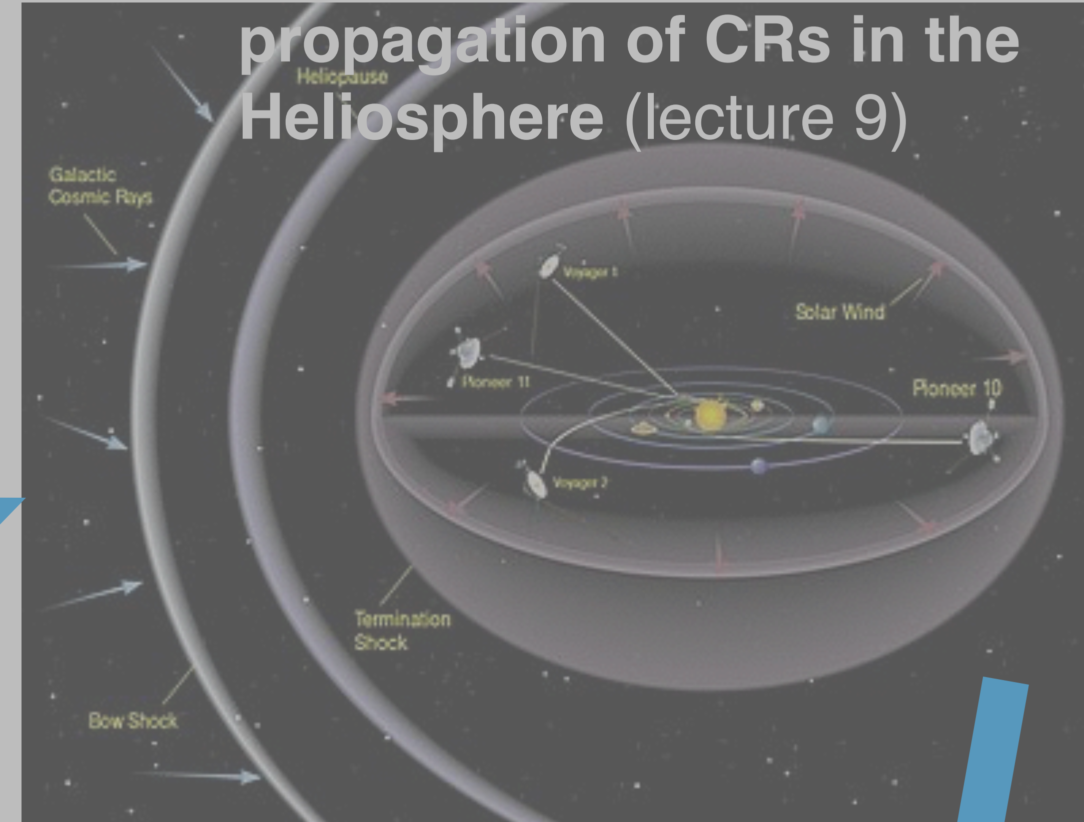

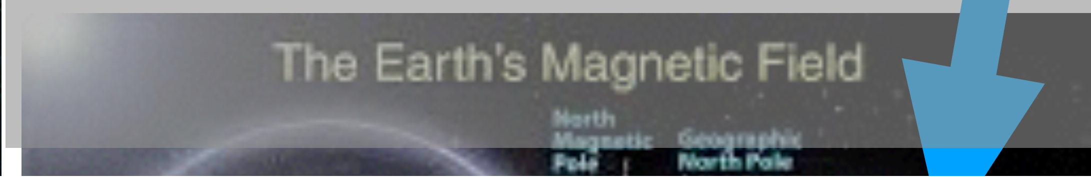

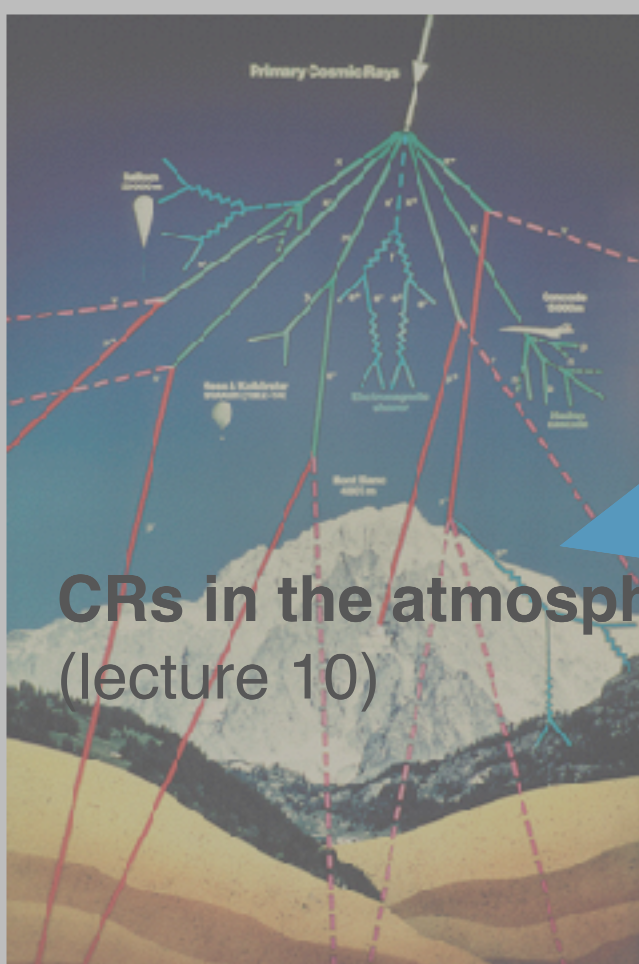

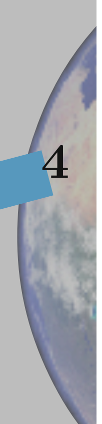

CRs a
atmos
10)

CRs underg
neutrino os

today:
Stanev, chapter 4

Cosmic rays in the Galaxy

Stanev chapter 4

After acceleration in SNRs cosmic rays propagate through the Milky Way.
The inter stellar matter (ISM) contains matter, B fields, and radiation fields.

Cosmic rays scatter at B fields and propagate in a diffusive process
—> cosmic rays arrive basically isotropic at the Earth
(recent measurements show some small anisotropy
—> will be discussed later)

Cosmic rays interact with matter in the ISM and produce secondary nuclei.

Electrons interact with radiation fields and B fields, as well as matter
in B fields they generate synchrotron radiation.
In radiation fields they boost gamma rays with the inverse Compton effect

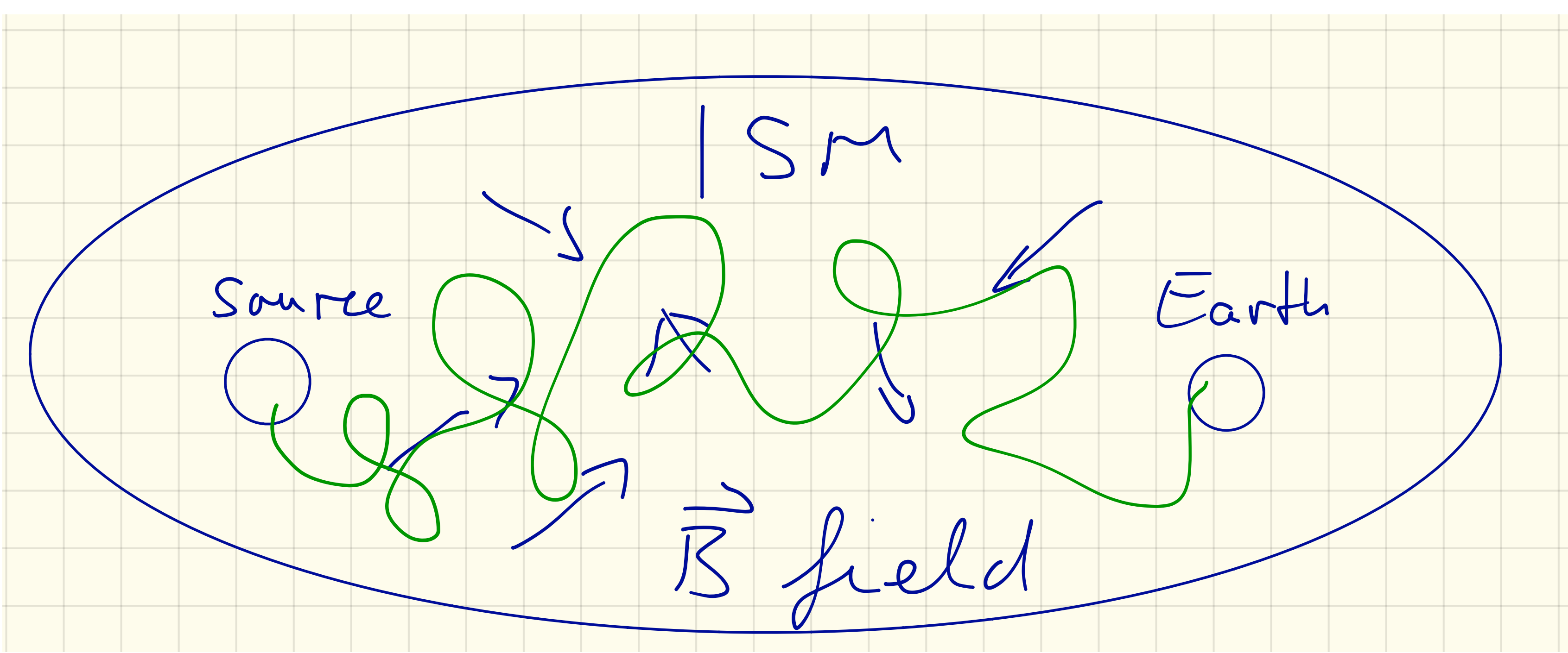

Luminous matter in Galaxy is organized in spiral arms

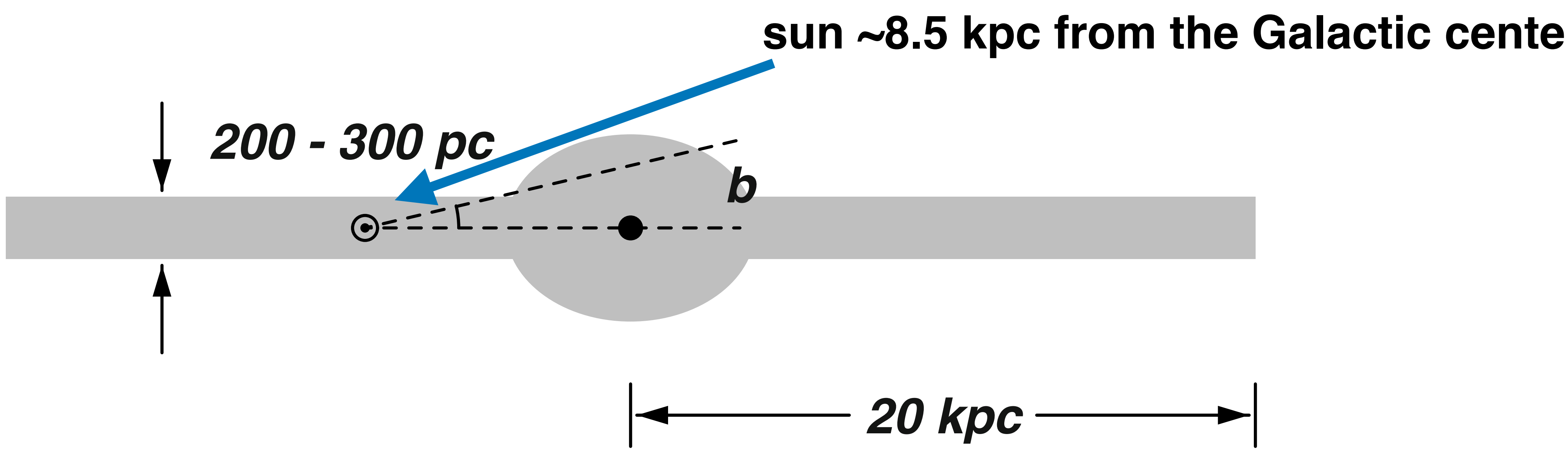

Fig. 4.1. View of the Galaxy from its side (not to scale). The black dot indicates the galactic center. The solar system is 8.5 kpc from the galactic center. In reality the galactic disk is much less regular than shown here.

Luminous matter in Galaxy is organized in spiral arms

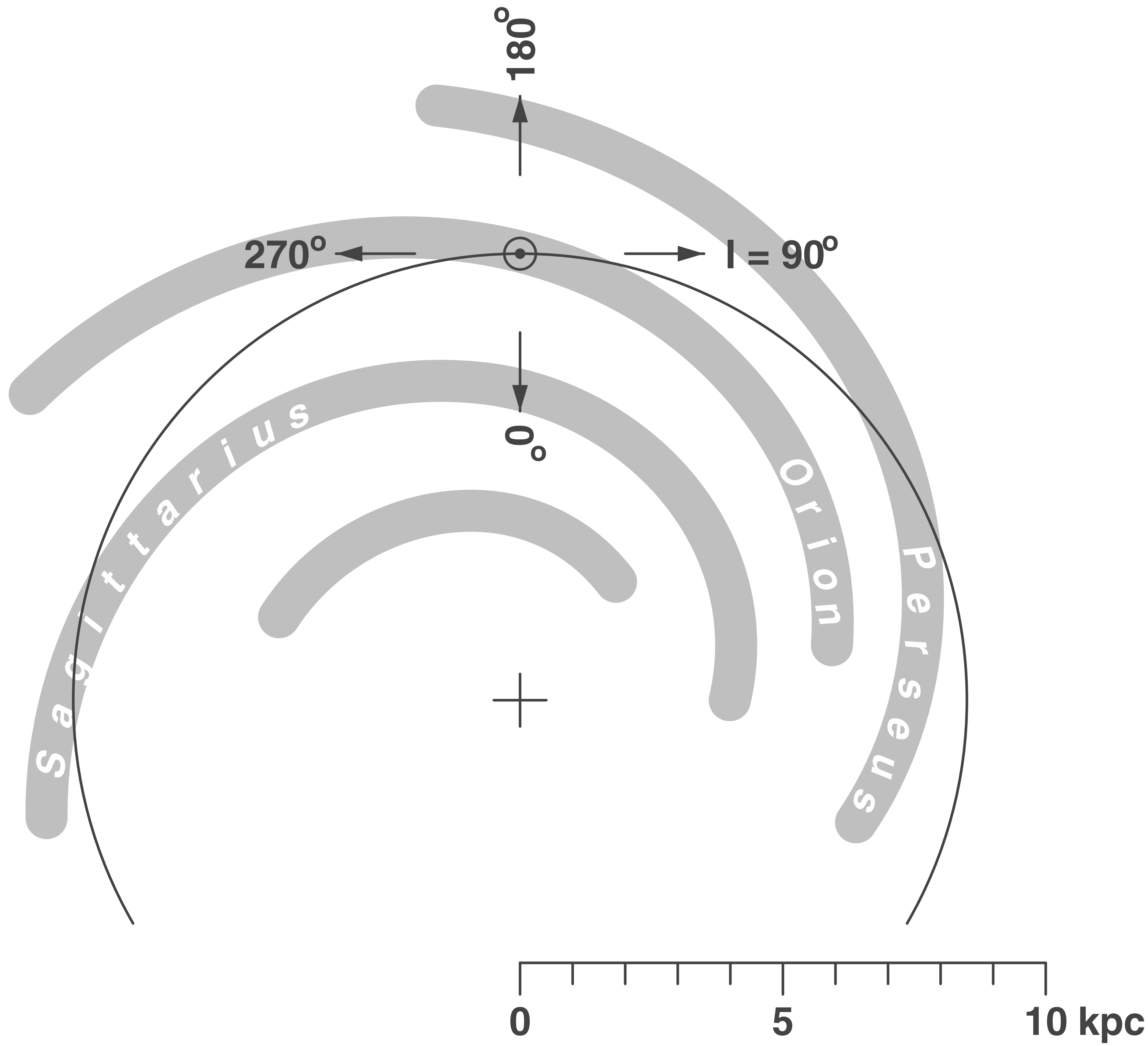

Fig. 4.2. View of the Galaxy from its North Pole. The galactic center is indicated with a cross. The galactic longitude ℓ is shown with arrows. The thin circle shows the solar circle.

Interstellar matter and magnetic field

Most of the diffuse ISM consists of hydrogen (only about 10% He and heavier nuclei) in the form of atomic hydrogen (HI) and molecular hydrogen (H_2).

HI is detected by its 21 cm emission line at radio frequencies
HI is present in Galactic arms
average density ~1 atom/cm^3
scale height ~100-150 pc

HI density about ~2 to 3 times less dense in space between arms

H_2 mostly within solar circle and in Galactic center
detected by 2.3 mm line of CO (acting as tracer for H_2)

total mass of H_2 within solar circle ~10^9 M_{sun}
average density within solar circle is then $$n(H_2) = \frac{10^9 M_\odot N_A}{V_{sc}} \simeq 1\ \mathrm{cm}^{-3}$$

for a full height of the Galactic disc of 200 pc and a volume of V_{sc} = 1.3 * 10^{66} cm^3

also ionized hydrogen has been detected density ~0.03/cm^3

good round number for ISM density 1 nucleon/cm^3
(real matter distribution very complicated)

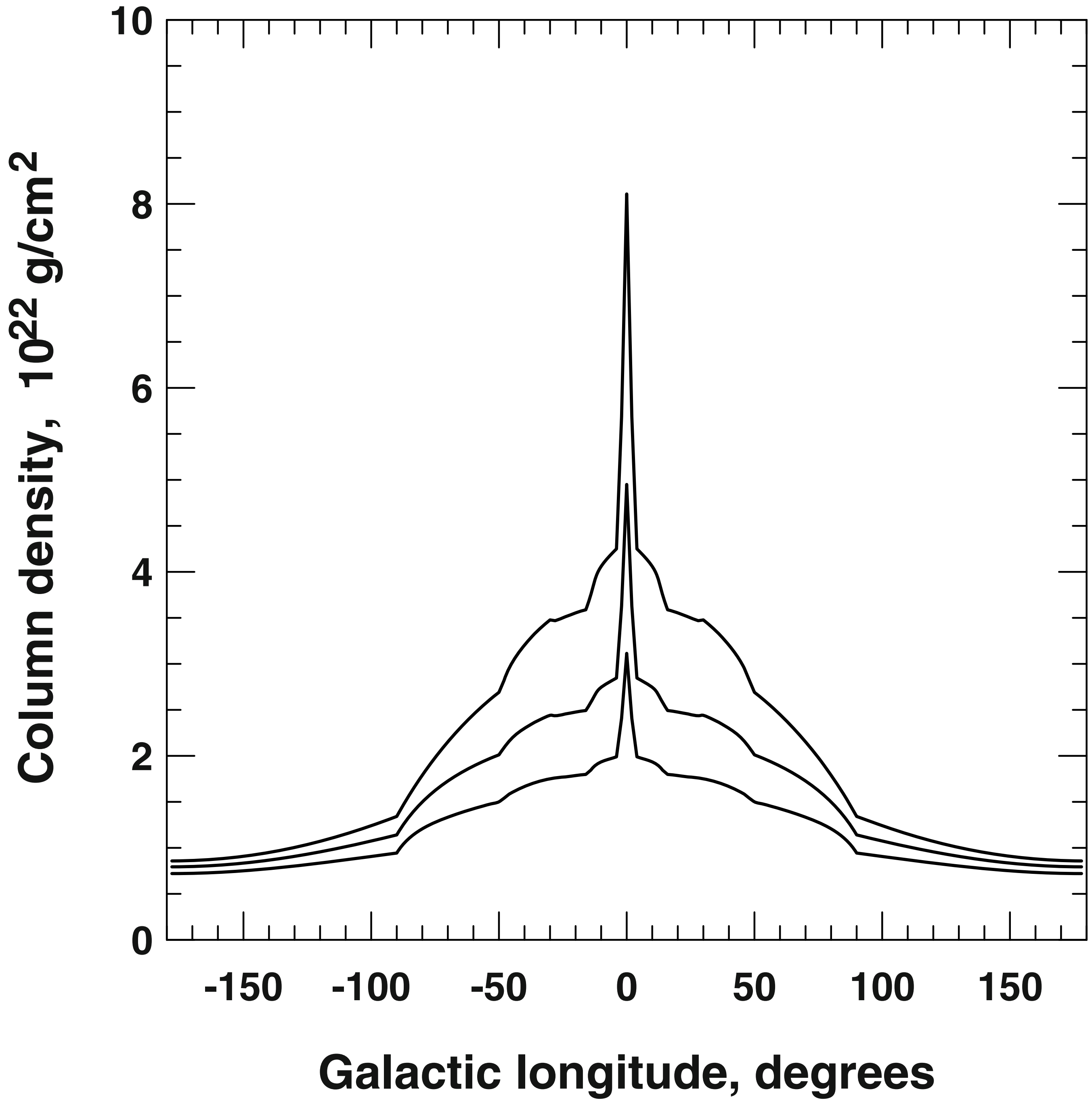

Fig. 4.3. Sketch of the column density of the Galaxy as a function of galactic longitude. The three lines are for longitudes within 2°, 5° and 10° from the galactic plane.

assuming cylindrical matter density in the Galaxy

B field in Galaxy

The magnetic field values are obtained from interpretations of the Faraday rotation of linearly polarized radio signals from radio pulsars. The rotation measure (rad/m^2) gives the integral of the product of the parallel component of the magnetic field and the electron density along the line of sight to the source, i.e.

$$RM = \int_0^d B_{||} n_e \, dr \, .$$

The electron density N_e has to be estimated by the delay of the arrival times of the radio signals as a function of the frequency – the dispersion measure of pulsars.

B field in the vicinity of the solar system ~3 μG

B field in Galaxy

The ideas of the large-scale structure are that the regular magnetic field follows the distribution of the matter, i.e. it has spiral form with either 2π (axisymmetric (ASS)) or π (bisymmetric (BSS)) symmetry. The bisymmetric model is currently favored, although axisymmetric models cannot be excluded. In bisymmetric models the field strength at a point (r, ϕ) in the galactic plane could be expressed (in polar coordinates) as [76]

$$\boxed{B(r,\phi) = B_0(r) \cos\left(\phi - \beta \ln \frac{r}{r_0}\right) ,} \tag{4.1}$$

where r_0 is the galactocentric distance of the position of the maximum field strength in the Orion arm, here assumed to be 10.55 kpc, and $\beta = 1/\tan p$. $B_0(r)$ could be taken as 2 μG at the position of the Sun and inversely proportional to the galactocentric distance, at least for $r > 4$ kpc [77]. Closer to the galactic center the field is higher, but its value is highly uncertain. The magnetic field strength and direction in the BSS model are shown in Fig. 4.4.

B field in Galaxy

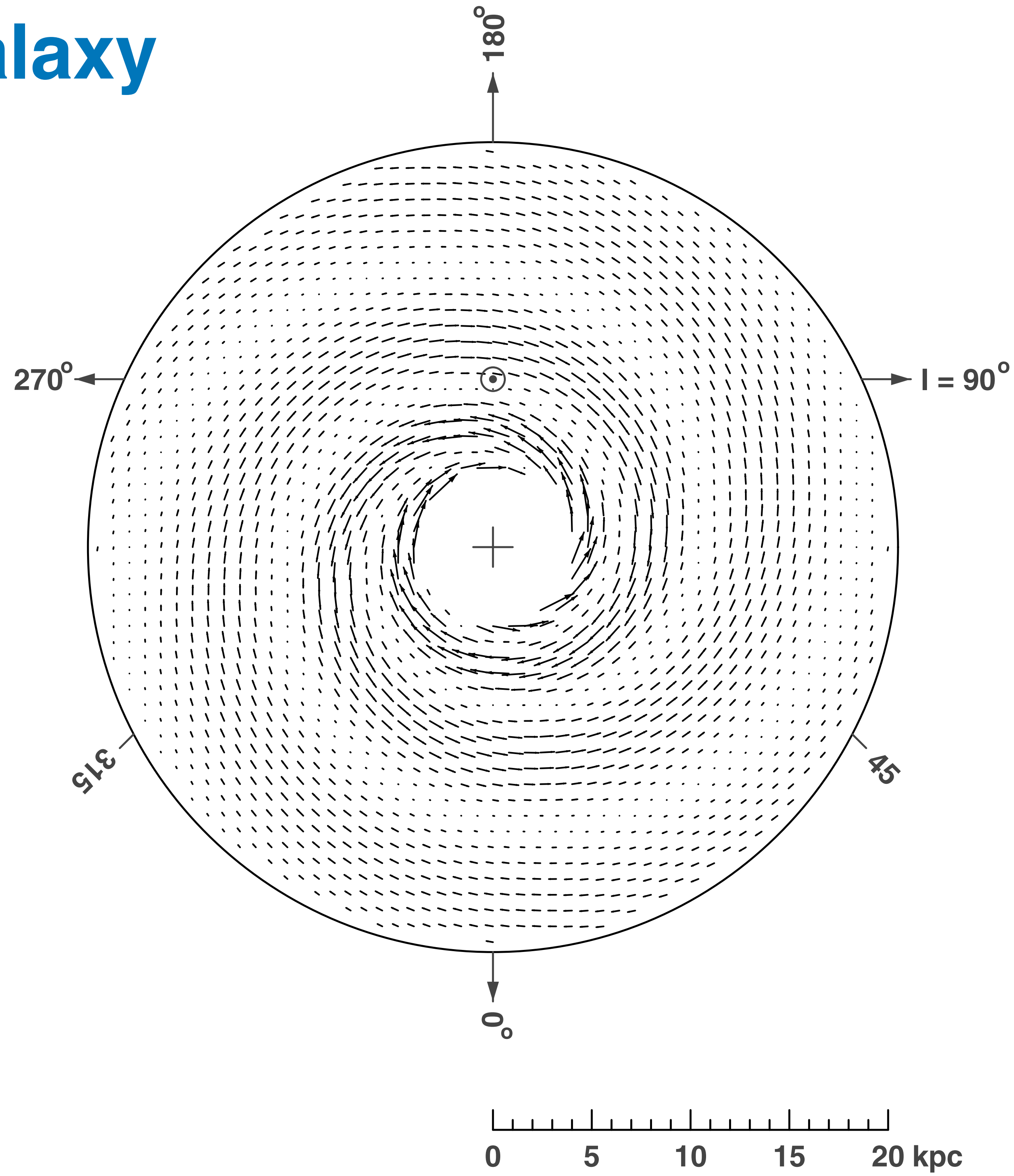

Fig. 4.4. Magnetic field strength (length of arrows) and direction in the galactic plane for the BSS model [76]. The field reversals can be best seen close to the galactic center where the field values are higher. The field is not plotted within 4 kpc of the galactic center because of the very high uncertainty in this region. The positions of the galactic center and the solar system are indicated.

Basic principles of the propagation

Ionized gas and B fields carried by it form a magnetohydrodynamic (MHD) fluid.
It supports waves that travel with the Alfvén velocity v_A.
CRs scatter on these waves during their propagation

The energy in MHD waves equals the energy density of the magnetic field, i.e.

$$\boxed{\frac{\rho v_A^2}{2} = \frac{B^2}{8\pi}\,.} \tag{4.4}$$

For an average field of 3 μG the energy density of the magnetic field is 4×10^{-13} erg/cm^3 $\simeq 0.25$ eV/cm^3 and is therefore somewhat smaller than the energy density of 0.5–1 eV/cm^3 carried by cosmic rays. Cosmic rays propagating in the interstellar medium must also induce Alfvén waves which in turn act as scattering centers.

Ginzburg & Syrovatskii [2] wrote the equation of cosmic rays transport in a general form. In their approach the production of cosmic rays in the Galaxy is described by the source term $Q_j(E,t)$. The source term $Q_j(E,t)$ is defined as the number of particles of type j produced (accelerated) per cm^3 at time t with energy between E and $E+\delta E$ in a given location in the Galaxy. These particles diffuse in the Galaxy and their number changes with time. The time evolution of the density $N_j(E,t)$ of cosmic rays of given type j and with energy E at a given location in the Galaxy is a function of the following five processes:

- Cosmic ray diffusion, characterized by the diffusion coefficient $\mathcal{K} = \beta c\lambda/3$ where λ is the diffusion mean free path and $v = \beta c$ is the particle velocity.
- Cosmic ray convection, characterized by the convection velocity v_c.
- The rate of change of the particle energy dE/dt. The energy change could be positive or negative. Negative dE/dt is provided by all forms of energy loss, and mostly by synchrotron radiation for the electrons or ionization loss for protons and heavier nuclei. Energy gain could be realized in 're-acceleration' processes, additional forms of acceleration during propagation in the galactic magnetic fields away from the original acceleration site.
- Particle loss term. Because of interactions or decays, particles of type j have turned into particles of type k and their number has to be subtracted from the density $N_j(E,t)$. The loss term is $p_j N_j(E,t)$, where $p_j = v\rho/\lambda_j + 1/\gamma_j\tau_j$ could be expressed as a function of the particle velocity v, interaction length λ_j and the target density ρ for the case of loss due to interactions and by its Lorentz dilated lifetime $\gamma_j\tau_j$ in the case of decay.
- Particle gain term. Because of interactions particles of type i have turned into particles of type j and have to be added to the density. This term is a weighted sum of all interactions and decays that create particles j.

All these processes affect the source term $Q_j(E,t)$ and give the particle density $N_j(E,t)$ as a function of time and energy.

general CR propagation principle

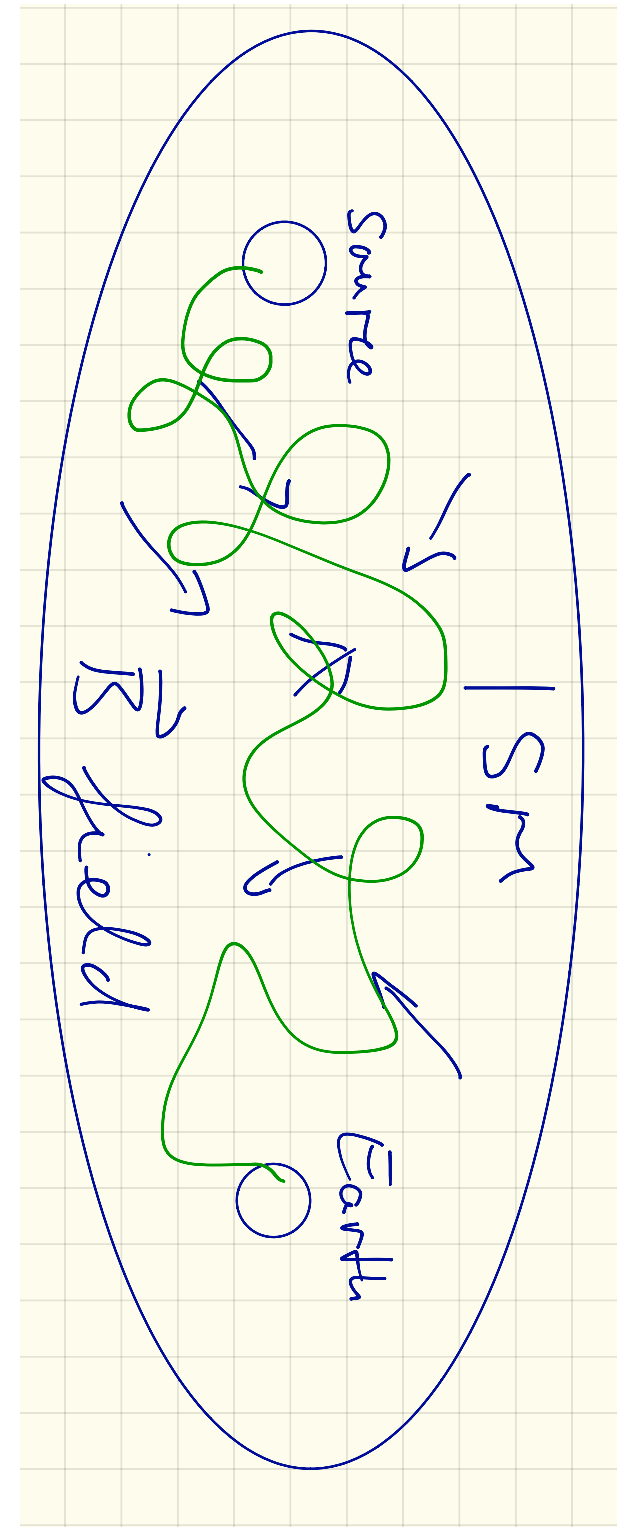

random walk

- in 1D, a random walker can move in either direction
- if it is isotropic, p(left)=p(right)
- the displacement after n steps of length l is

$$x(n) = \sum_{i=1}^{n} s_i \qquad\qquad s_i = \pm\, l$$

- the average displacement is

$$\langle x(n) \rangle = \langle \sum_{i=1}^{n} s_i \rangle \sim 0$$

- the rms of the displacement is

$$\langle x^2(n) \rangle = \langle \sum_{i=1}^{n} s_i^2 \rangle = l^2 n$$

- the isotropic case is easy, as it can be simulated by generating random numbers r in [0,1], and associating, for instance, r>0.5 with left and r<0.5 with right

- in the anisotropic case, we associate p with the probability of the particle to go left, and q=1-p with the probability to go right
- after n steps, a particle will have displaced k=i-j, where i is the number of steps to the left, and j the number os steps to the right
- the probability of finding k is

$$P(k) = \frac{\text{number of (i,j) arrangements}}{\text{total number of arrangements}} = \frac{\frac{n!}{i!j!}}{2^n} = \frac{n!}{2^n \left(\frac{n+k}{2}\right)!\left(\frac{n-k}{2}\right)!}$$

Stirling expansion: $\ln(x!) = x \ln x - x$

rewriting the probability:

$$\ln(P(k)) = n \ln n - \frac{1}{2}\left[(n+k)\ln(n+k) + (n-k)\ln(n-k)\right] \approx -\frac{k^2}{2n}$$

$$P(k) = \exp\left(-\frac{k^2}{2n}\right)$$

- in the continuous case, x=kλ, so the probability becomes

$$P(x) = A \exp\left(-\frac{x^2}{2n\lambda^2}\right) = \frac{1}{\sqrt{2\pi n\lambda^2}} \exp\left(-\frac{x^2}{2n\lambda^2}\right)$$

- because x, y, z are independent, the probability for a 3D random walk is simply the product of P(x)P(y)P(z):

$$P(x,y,z) = \frac{1}{(2\pi n\lambda^2)^{3/2}} \exp\left(-\frac{x^2+y^2+z^2}{2n\lambda^2}\right)$$

$$P(r) = \frac{4\pi}{(2\pi n\lambda^2)^{3/2}} \exp\left(-\frac{r^2}{2n\lambda^2}\right) r^2$$

- defining the number of "collisions" [idea will be generalised latter]: $n_i=\Gamma t$:

$$P(r) = \frac{4\pi}{(2\pi \Gamma t\lambda^2)^{3/2}} \exp\left(-\frac{r^2}{2\Gamma t\lambda^2}\right) r^2$$

- we can now define a coefficient that describes how a particle moves, the diffusion coefficient

$$D \equiv \frac{1}{2}\Gamma\lambda^2$$

so that the probability becomes

$$P(r) = \frac{4\pi}{(4\pi D t)^{3/2}} \exp\left(-\frac{r^2}{4Dt}\right) r^2$$

- now the mean and rms values of r can be computed

$$\langle r \rangle = \int_0^\infty P(r) r dr = 0 \qquad \langle r^2 \rangle = \int_0^\infty P(r) r^2 dr = 6Dt$$

- now the mean and rms values of r can be computed

Bohm diffusion

In the case of three-dimensional diffusion the r.m.s. distance of a particle to its source increases as

$$\langle r^2 \rangle \simeq 2\mathcal{K}t \,, \tag{4.9}$$

where t is the diffusion time and $\mathcal{K}$ is the diffusion coefficient ($\mathcal{K} = (3c/2) \times (r_g^2/l_{coh})$), i.e. for a relativistic particle moving with velocity c the diffusion length $\lambda = r_g^2/2l_{coh}$. Since l_{coh} depends only on the random field, the diffusion length is a strong function of the particle energy.

A special case of the fastest possible diffusion is the *Bohm diffusion* where the mean free path (l_{coh}) approaches the particle gyroradius r_g. The diffusion coefficient for *Bohm diffusion* is $\mathcal{K}_\mathrm{B} = cr_g/3$. One can use $\mathcal{K}_\mathrm{B}$ to set a limit for the distance particles of energy E can diffuse for time t. For random galactic fields it follows from (4.9) that for protons of energy E GeV

$$\boxed{\sqrt{\langle r^2 \rangle} \simeq 5\,\mathrm{pc} \times \left[\frac{3 \times 10^{13} \times E}{\mu G} \frac{\tau_G}{10^9\ \mathrm{yrs}} \right]^{\frac{1}{2}}} \tag{4.10}$$

where μG is the average strength of the random galactic fields and τ_G is the age of the Galaxy. Equation (4.10) gives the average distance to which protons of energy E GeV diffuse. Since *Bohm diffusion* is an upper limit for $\mathcal{K}$ the real absolute limiting diffusion distance is larger.

Formation of the chemical composition

Relative abundance of elements at Earth

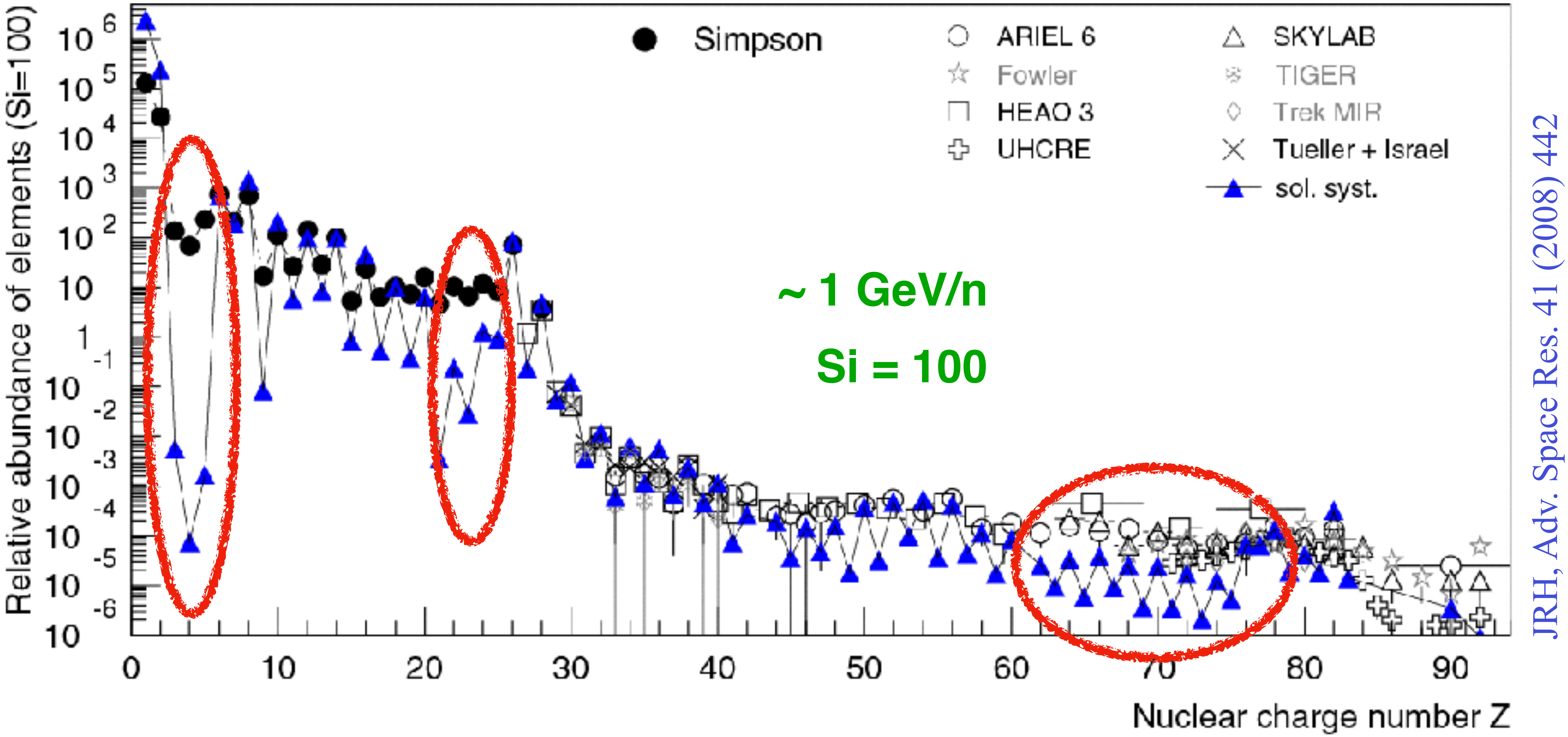

abundance of elements in CRs and solar system mostly similar

but few differences, e.g. Li, Be, B —> important to understand propagation of cosmic rays in Galaxy —> column density of traversed matter

primary cosmic rays generated at source e.g. p, He, Fe
spallation products —> secondary cosmic rays, e.g. Li, Be, B

Leaky box approximation

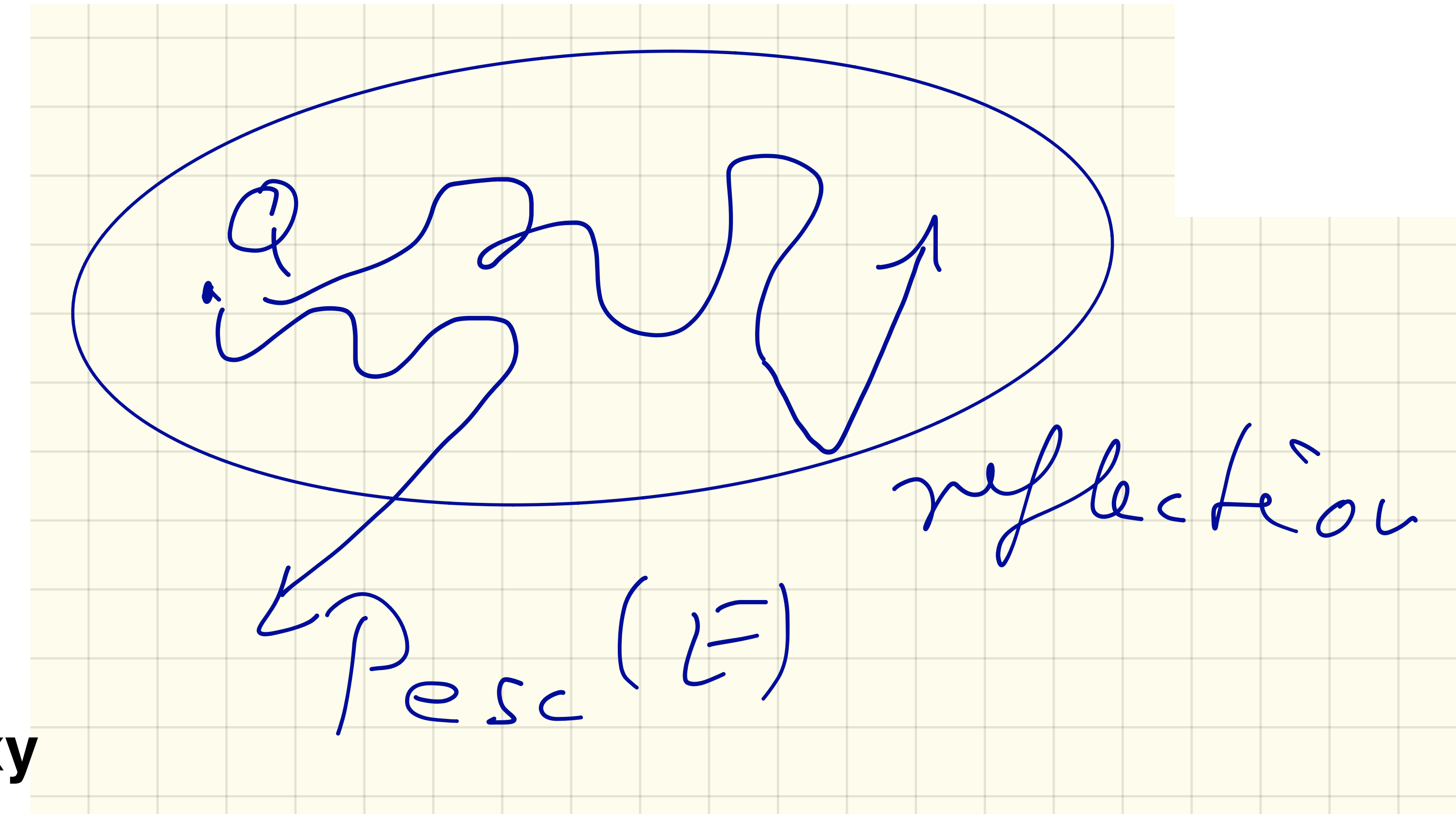

free propagation of CRs in a closed volume (Galaxy)

energy dependent escape probability $P_{esc}(E)$, **constant in time**

λ_{esc}, **mean amount of matter traversed by CRs in the Galaxy**

$$\lambda_{esc} \equiv \rho_{ISM} \beta c \tau_{esc},$$

τ_{esc} **life time/residence time of CRs in the Galaxy**

simplified transport equation for stable CR nuclei

(neglecting energy loss and gain)

$$\frac{N_j(E)}{\tau_j(E)} = Q_j(E) - \frac{\beta c\, \rho_{ISM}}{\lambda_j(E)} N_j(E) + \frac{\beta c\, \rho_{ISM}}{m} \sum_{i>j} \sigma_{i \to j} N_i(E)\,. \qquad (4.11)$$

The negative term on the right-hand side of the equation describes the number of nuclei of type j lost in propagation because of fragmentation. The positive term sums over all higher mass nuclei that produce j in spallation processes.

Formation of the chemical composition

The observed cosmic ray composition can be understood in terms of the general elemental abundance and the fragmentation cross-sections if all cosmic ray nuclei have the same propagation history [83, 84] and have on the average traversed 5 to 10 g/cm^2 of matter. For ρ_{ISM} of one nucleon per cm^3 this corresponds to escape time $\tau_{esc} = N_A \lambda_{esc}/c \simeq 3\text{–}6 \times 10^6$ years.

The study of the energy dependence of the secondary to primary ratio establishes the energy dependence of the containment time for cosmic rays in the Galaxy. Using measurements like the one shown in Fig. 4.6 one could fit the energy dependence of λ_{esc} as [82]

$$\boxed{\lambda_{esc} = 10.8\,\beta \times \left(\frac{4}{R}\right)^{\delta} \text{g/cm}^2\,,} \tag{4.12}$$

where R is the particle rigidity in GV and $\delta \simeq 0.6$ shows the rigidity dependence of the escape length. The formula is valid for rigidities above 4 GV. At lower rigidities the escape length is almost constant at $\lambda_{esc} = 10.8\beta$ g/cm^2.

Current B/C measurements (AMS-02 red points)

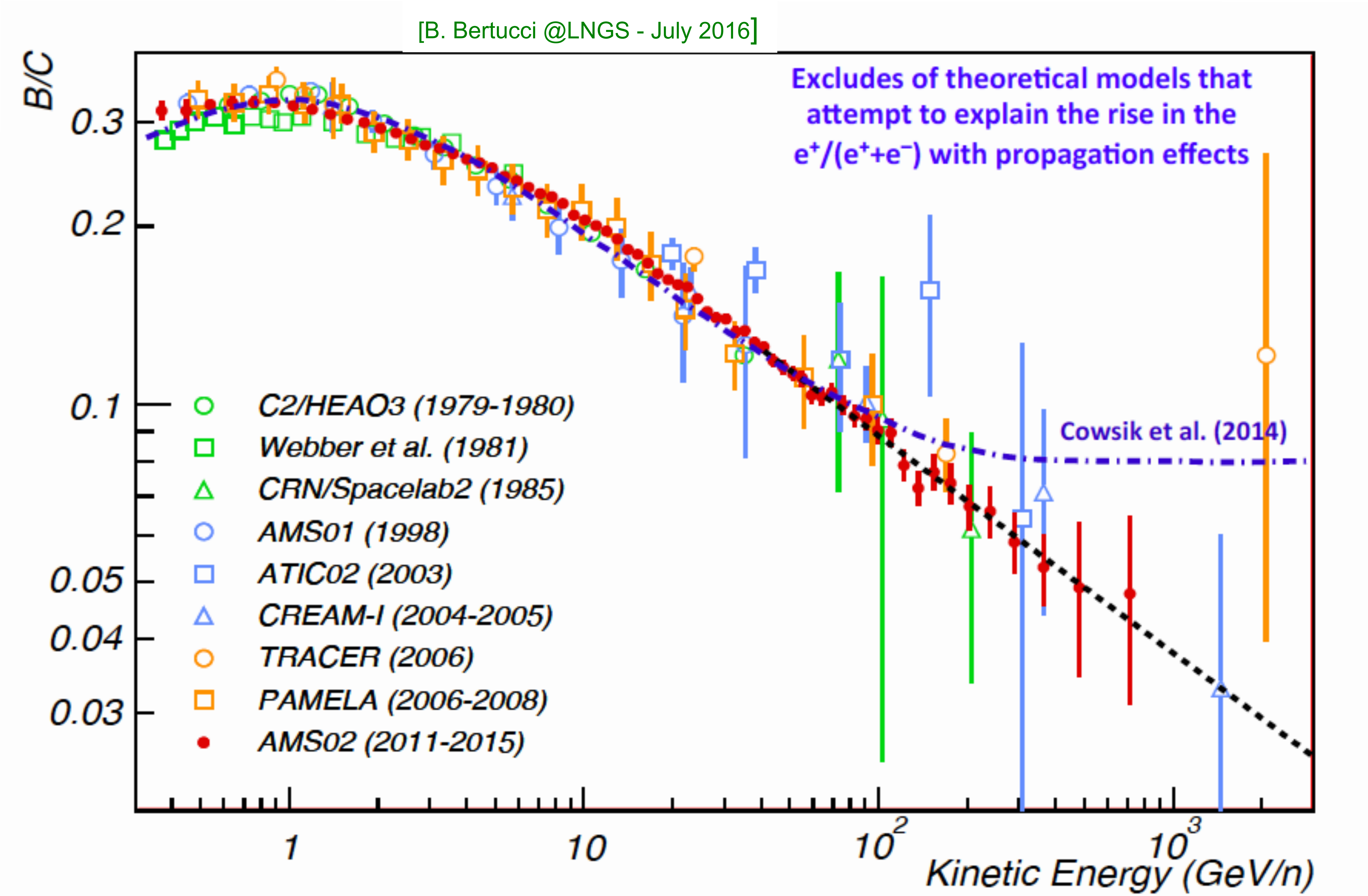

ECRS 2016 Torino, *September 7, 2016*

P. S. Marrocchesi

If we make one more simplification and assume that no cosmic ray nuclei are created in propagation, i.e. only account for the loss of particles, the leaky box model gives the shape of the energy spectrum of a primary nucleus j after propagation as

$$\boxed{N_j(E) = Q_j(E) \times \left(\frac{1}{\tau^j_{esc}(E)} + \frac{\beta c \rho_{ISM}}{\lambda^j_{int}} \right)^{-1}}, \tag{4.13}$$

where $Q_j(E)$ is the source spectrum for the nucleus j. While the escape length $\lambda_{esc}(E)$ is the same for all nuclei with the same rigidity R, λ_{int} depends on the mass of the nucleus. In the case of protons λ_{int} is the cross-section for inelastic interactions – 50.8 g/cm^2 at low energy. For heavier nuclei, interactions also include fragmentations. λ_{int} is 6.4 g/cm^2 for carbon and only 2.6 g/cm^2 for iron. Equation (4.13) suggests that the energy spectra of different nuclei will be different at low energies and will tend to become asymptotically parallel to each other at high energy if they were accelerated to the same spectral index at source. Figure 4.7 shows the modification of the source spectra of carbon and iron as a function of their energy and with escape length given by (4.12). Note that the smaller λ_{int} is, the bigger the modification of the source spectrum will be. In the case of protons, λ_{esc} is always smaller than λ_{int} and the modification is simply a steepening of the acceleration spectrum from $E^{-\alpha}$ at acceleration to $E^{-(\alpha+\delta)}$ after propagation. For $\delta = 0.6$ this would suggest an acceleration spectrum with $\alpha = 2.1$ to fit the $E^{-2.7}$ observed energy spectrum of cosmic rays.

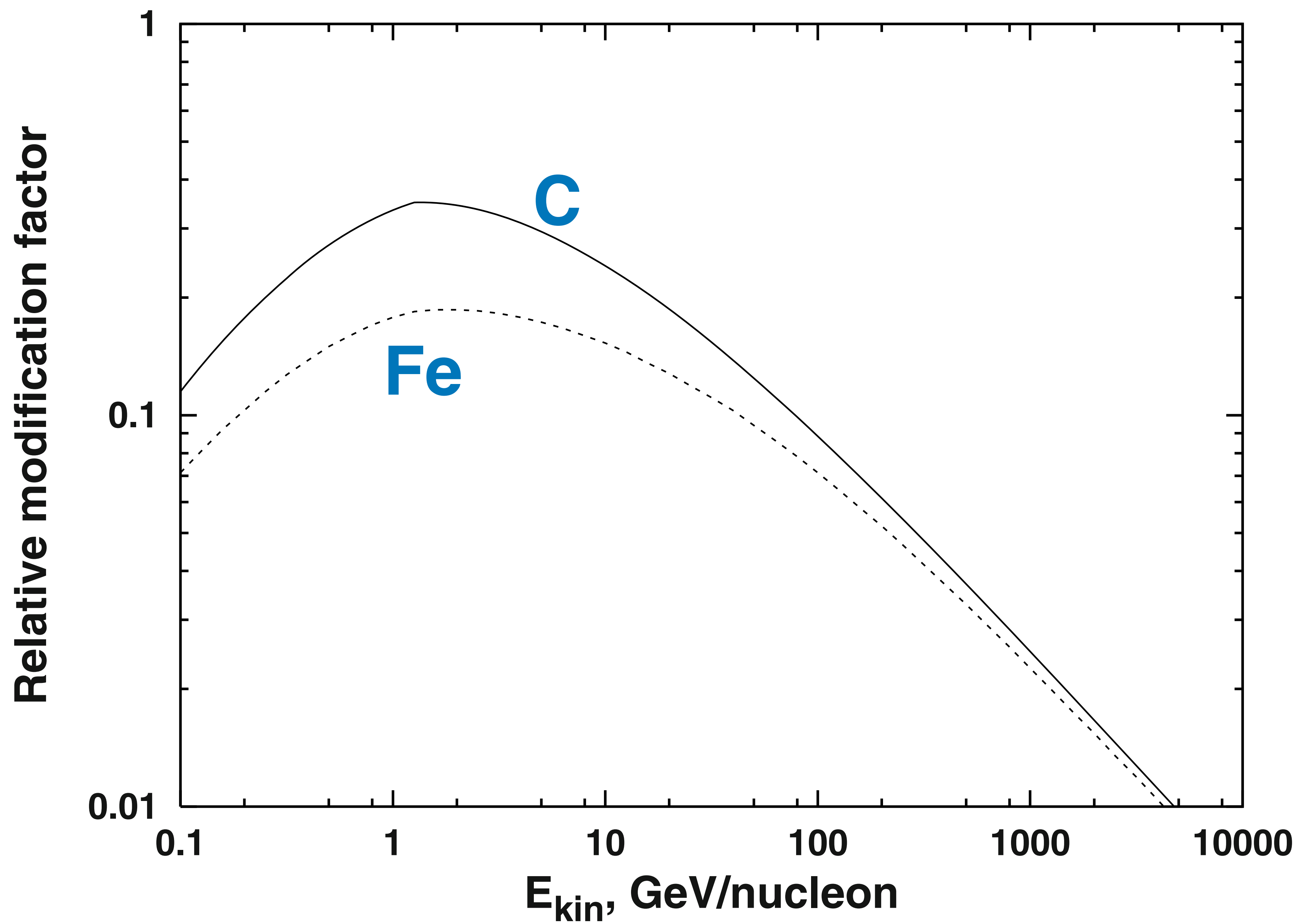

Fig. 4.7. Modification of the shape of the energy spectrum of carbon (solid line) and iron (dashed line) nuclei after propagation on the assumption of no particle gain. Only the relative shape of the spectrum of the two nuclei is correct, because the normalization depends on the average interstellar density during propagation.

Shape of energy spectrum

$$\frac{dN}{dE} \propto E_0^{\gamma}$$

at source γ ~ -2.1

at Earth γ ~ -2.6 to -2.7

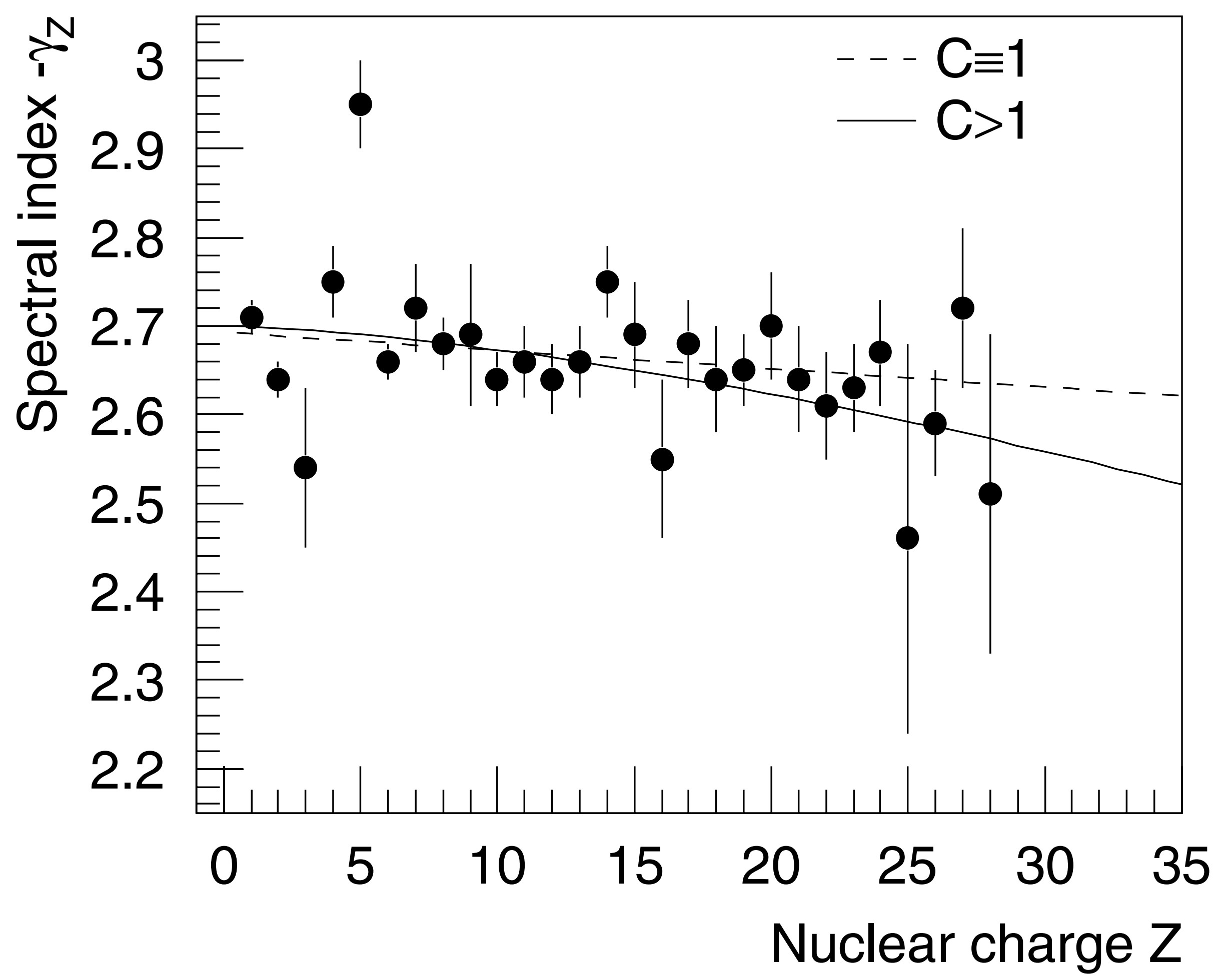

Fig. 5. Spectral index γ_Z versus nuclear charge Z (see Table 1). The solid line represents a three parameter fit according to Eq. (6), the dashed graph a linear fit.

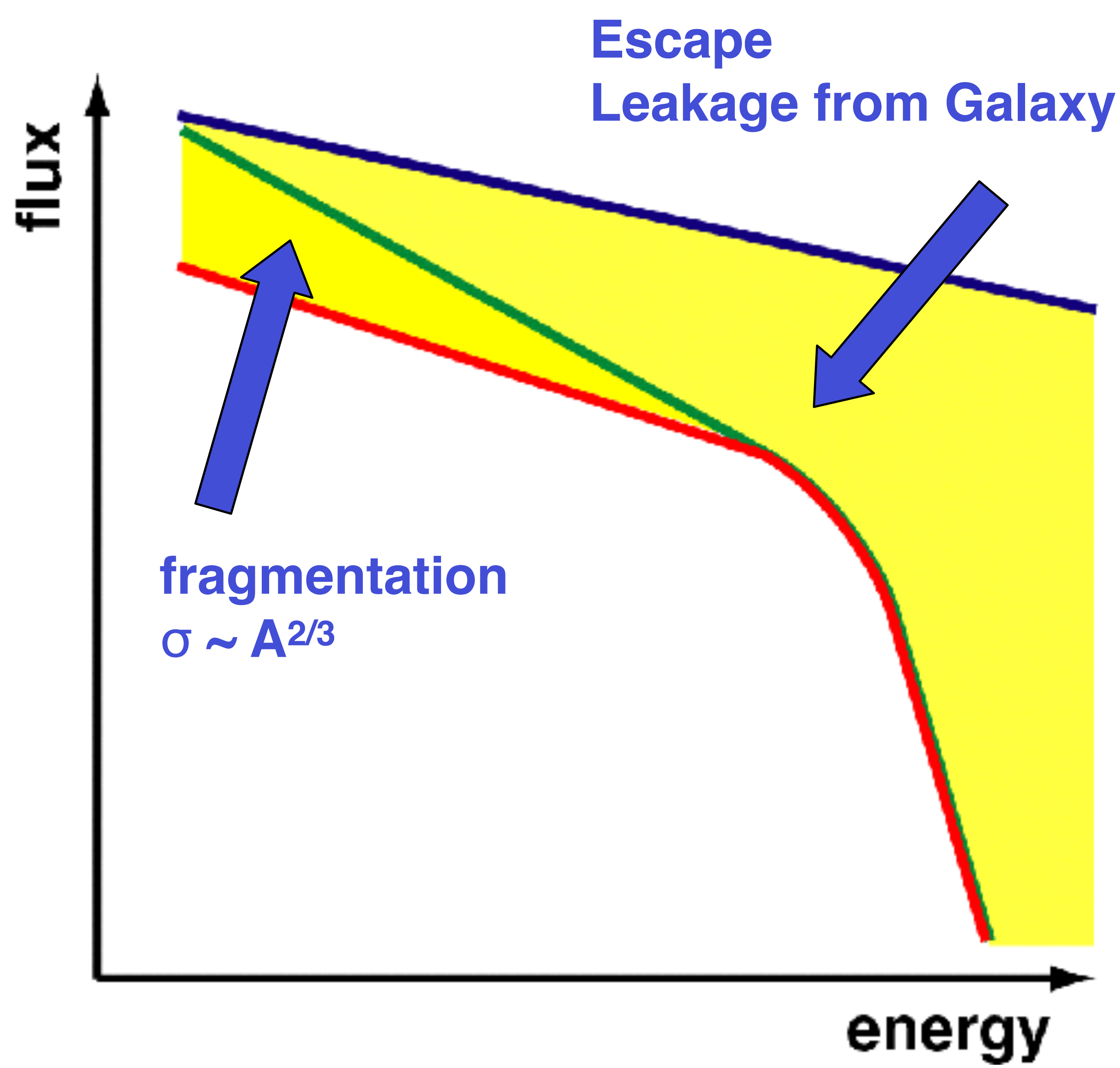

JRH, Astropart. Phys. 19 (2003) 193

Life time of CRs in Galaxy

In principle the problem of the containment volume could be solved by observations of non-stable secondaries that decay with a half life comparable to the escape time of cosmic rays. To do this one has to put back the decay length in the negative term of (4.11), which becomes

$$\boxed{\left(\frac{\beta c \rho_{ISM}}{\lambda_j(E)} + \frac{1}{\gamma \tau_j}\right) \times N_j(E)\ .}$$

A very suitable isotope is ^{10}Be with a half life of 1.6×10^6 years. The flux of ^{10}Be can be compared with the stable isotopes ^{9}Be and ^{7}Be. The production of the three isotopes depends on the partial production cross-sections and on λ_{esc}. ^{10}Be would decay and its measured flux depends also directly on τ_{esc}. The actual estimate involves folding of the production with the decay of the isotope during propagation in a particular propagation model. The measurements are also very difficult and the results from their analysis are not fully conclusive.

Chart of the nuclides

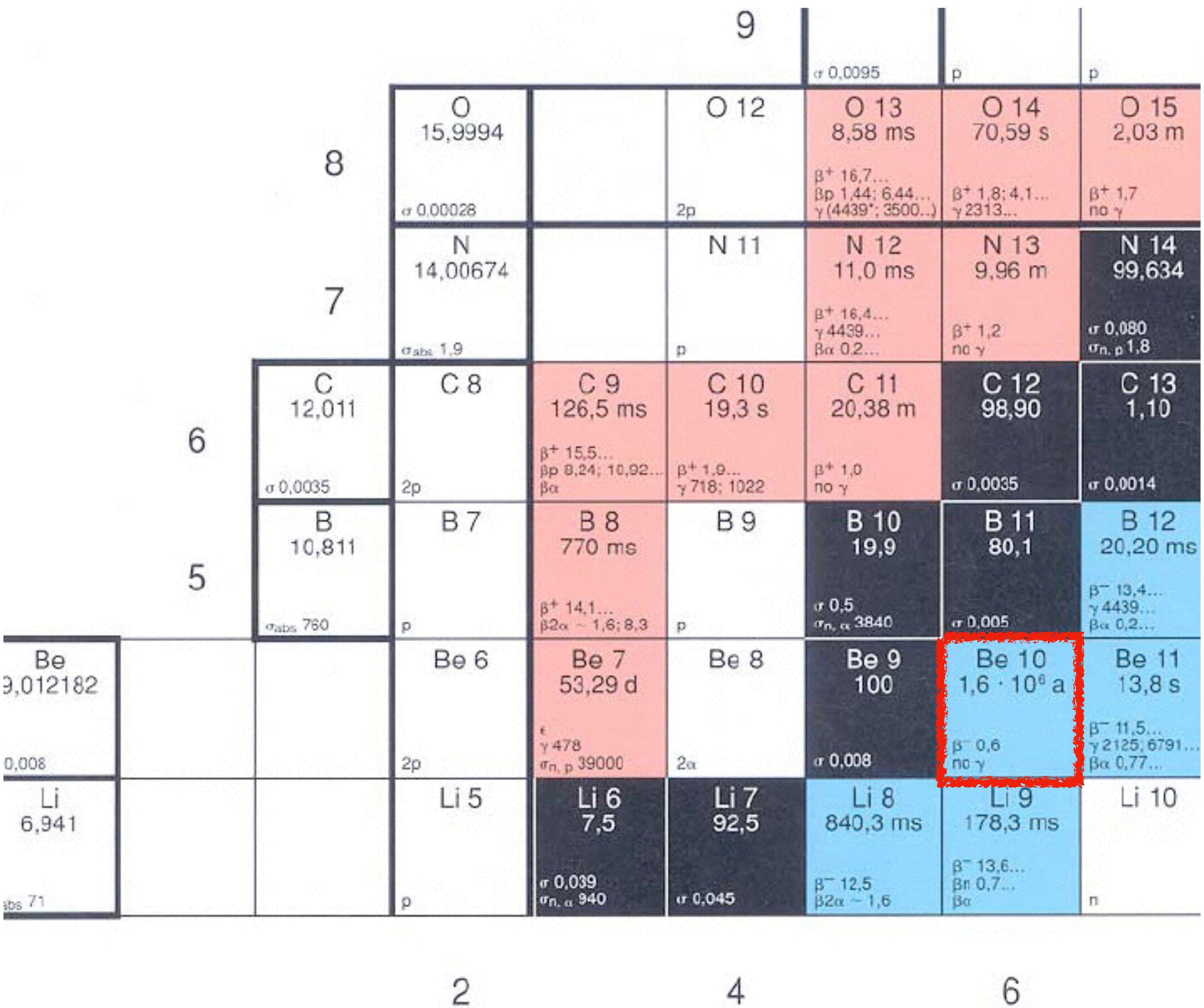

THE ASTROPHYSICAL JOURNAL, 217:859–877, 1977 November 1

„Age" of galactic cosmic rays

THE AGE OF THE GALACTIC COSMIC RAYS DERIVED FROM THE ABUNDANCE OF ^{10}Be*

M. GARCIA-MUNOZ, G. M. MASON, AND J. A. SIMPSON†
Enrico Fermi Institute, University of Chicago
Received 1977 March 14; accepted 1977 April 21

Residence time in Galaxy

$^{10}\mathrm{Be} \rightarrow {}^{10}\mathrm{B} + e^-$ (t =2.4 10^6 a)

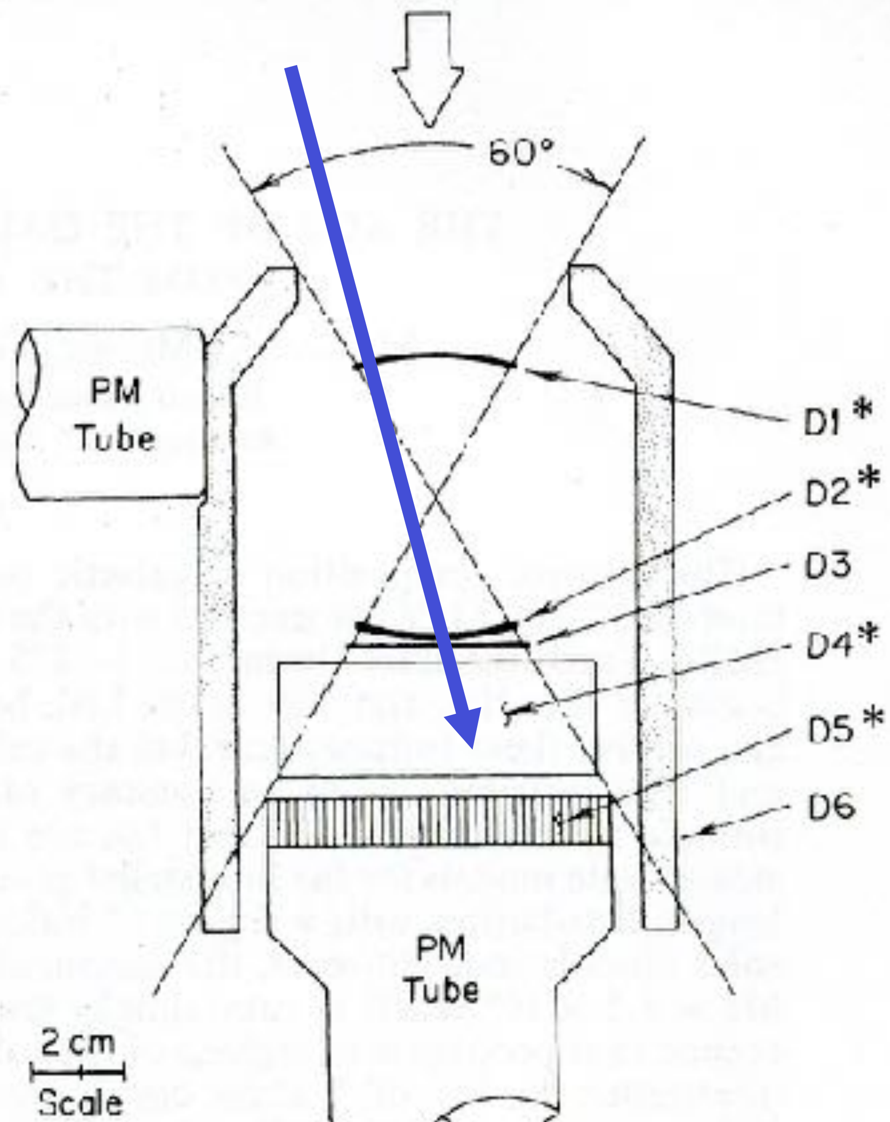

FIG. 1.—Cross section of the IMP-7 and IMP-8 telescopes. D1, D2, and D3 are lithium-drifted silicon detectors of thickness 750, 1450, and 800 μm, respectively. D4 is an 11.5 g cm^{-2} thick CsI (Tl) scintillator viewed by four photodiodes. D5 is a sapphire scintillator/Cerenkov radiator of thickness 3.98 g cm^{-2}, and D6 is a plastic scintillation guard counter viewed by a photomultiplier tube. Asterisks denote detectors whose output is pulse-height analyzed.

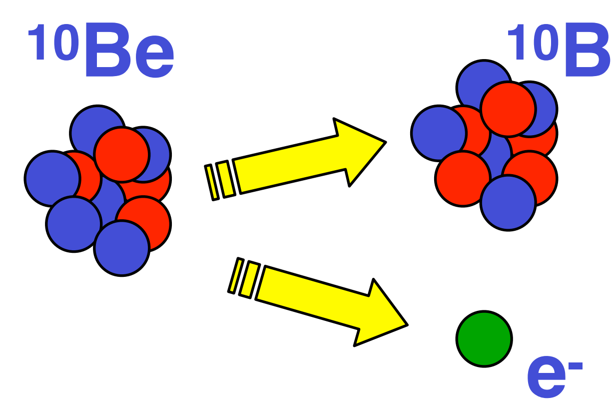

latest measurement from ACE/CRIS experiment:

$$\tau_{esc} = 17 \cdot 10^6 \text{ a}$$

$$\Rightarrow \tau_{esc} = 17 \cdot 10^{6}\ \mathrm{a}$$

from this, we can derive an average density

$$\bar{\rho} = \frac{\lambda_{esc}}{v \cdot \tau_{esc}} = \frac{10\ \mathrm{g/cm^2}}{3 \cdot 10^{10}\ \frac{\mathrm{cm}}{\mathrm{s}} \cdot 17 \cdot 10^{6} \cdot 86400 \cdot 365\ \mathrm{s}}$$

$$= 0{,}3\ \mathrm{H\ atom/cm^3}$$

galaxy

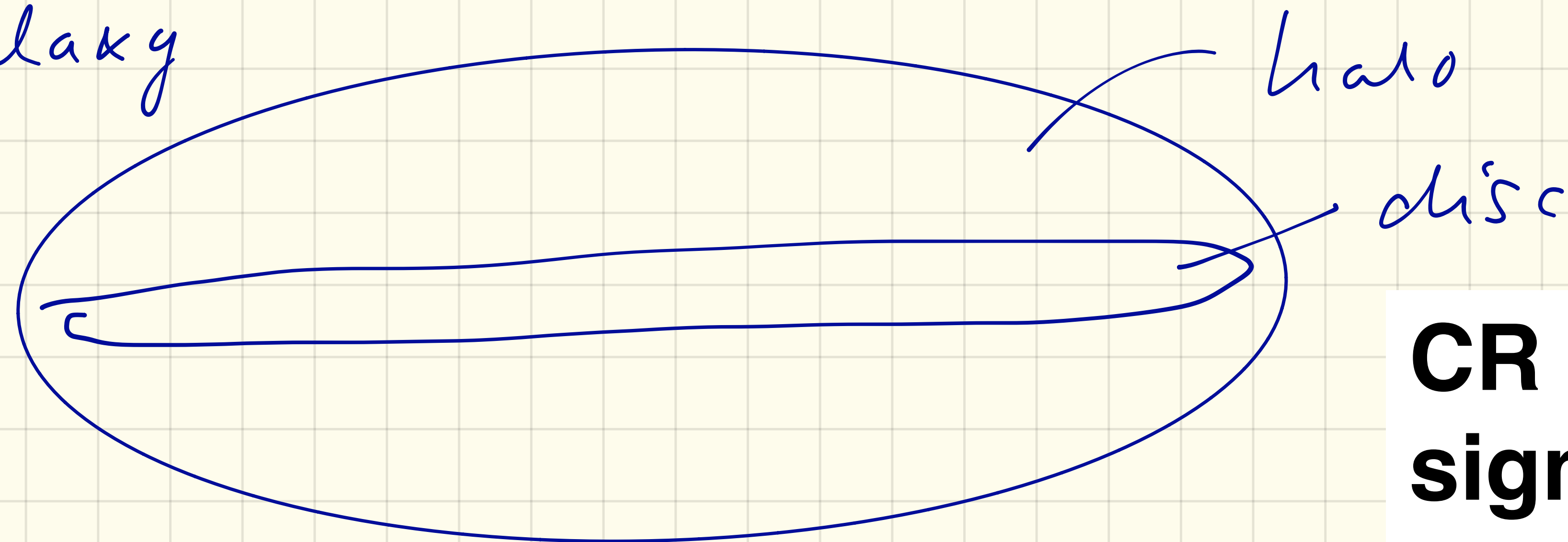

CR particles spend a significant fraction of their residence time in the Galactic halo (lower density)

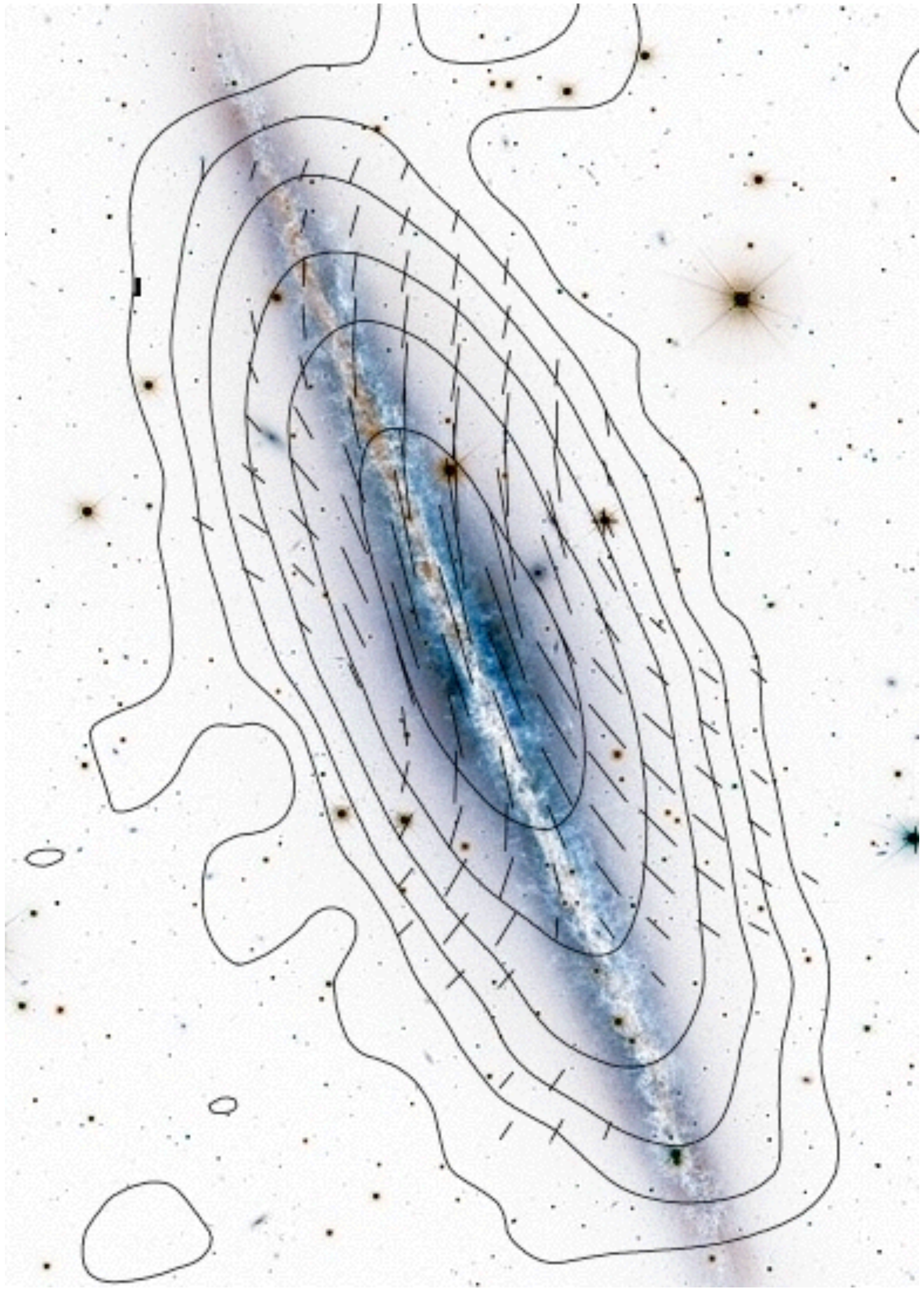

confirmed by observations of diffuse radio emission

synchrotron radiation

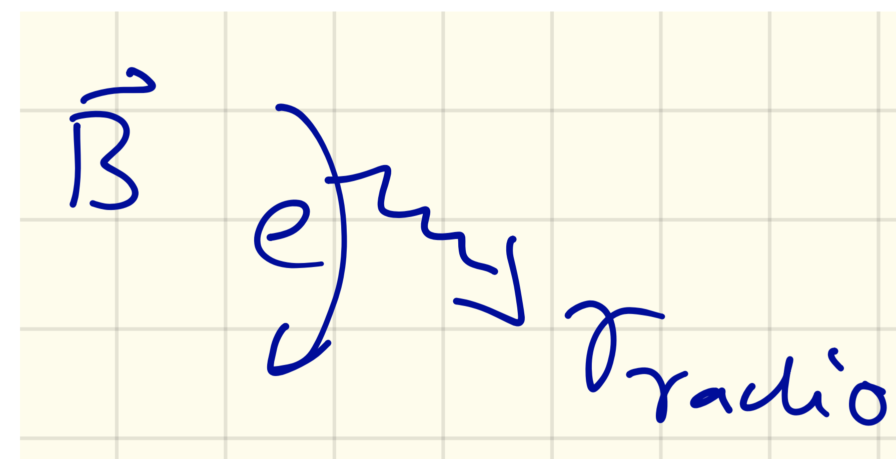

This figure shows the spiral galaxy **NGC 891**, seen almost edge-on, which is believed to be very similar to our Milky Way. It was observed at 8.4 GHz (3.6 cm wavelength) with the Effelsberg 100m telescope. The background optical image is from the CFHT Observatory. The "X-shaped" structure of the magnetic fields indicates the action of a galactic wind. The observed extent of the radio halo is limited by the large energy losses of the cosmic-ray electrons emitting at this wavelength. At lower frequencies (longer wavelengths) the radio waves are emitted by electrons with lower energies for which the energy lossesare smaller, so that larger radio halos are expected.

diffuse radio background of the Milky Way

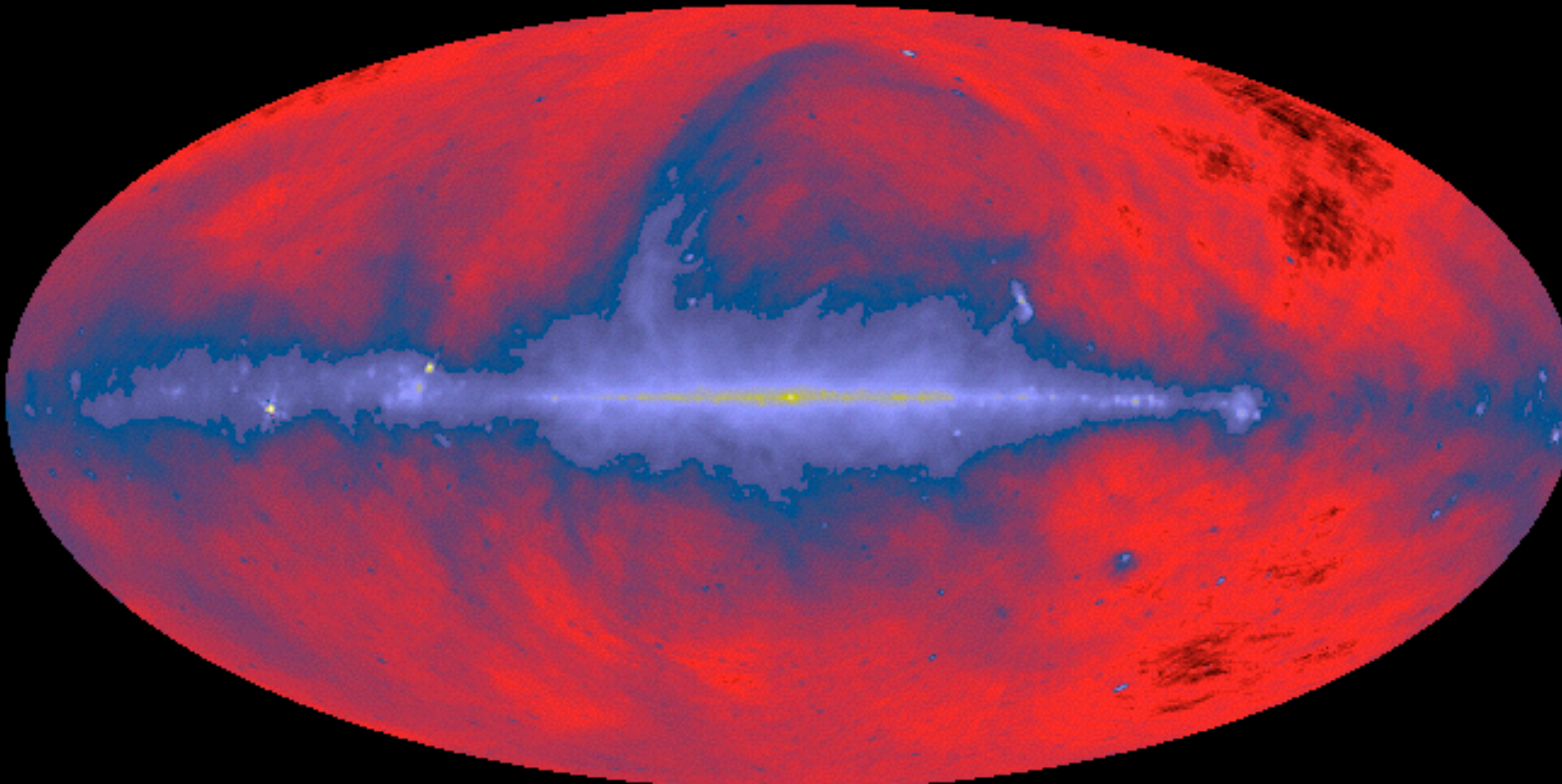

radio wavelengths

synchrotron radiation from electrons in B fields

intensity $\propto B\rho_e$

halo of galaxies are more extended than the visible region

--> confirmation that cosmic rays (electrons)

propagate in the galactic halo

Diffuse Galactic gamma rays

diffuse gamma radiation observed E>100 MeV
origin: $CR + ISM \rightarrow \pi^0 \rightarrow \gamma + \gamma$

--> direct hint that cosmic rays (hadrons) are not a local phenomenon
they propagate in the halo of the Milky Way and they exist in other galaxies

electrons produce gamma rays through *bremsstrahlung* and *inverse Compton interaction* with CMB and with diffuse infrared/optical radiation

The Fermi All Sky Map, showing the diffuse galactic gamma-ray background from the Milky Way.

Courtesy of NASA/DOE/International LAT Team

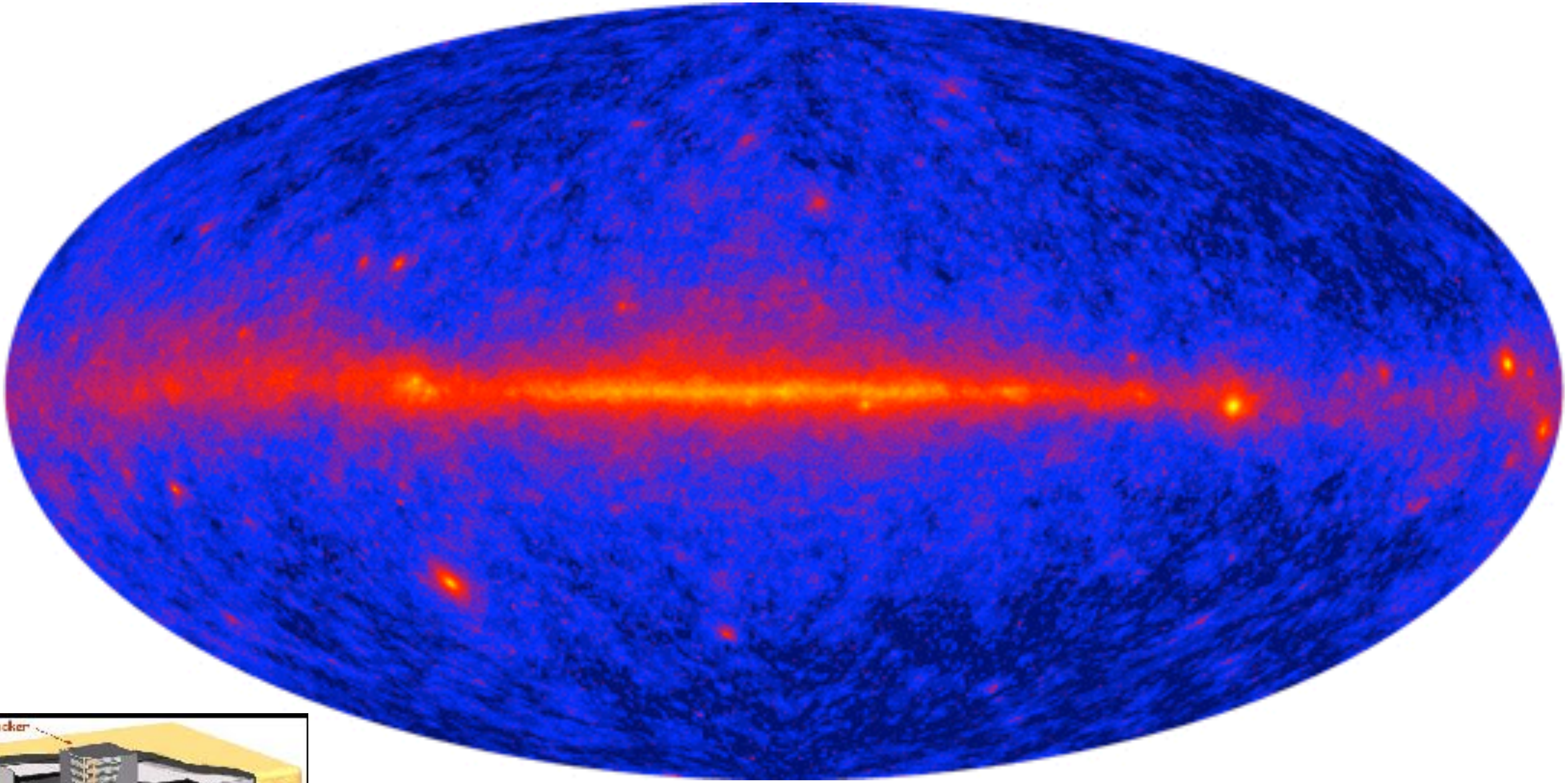

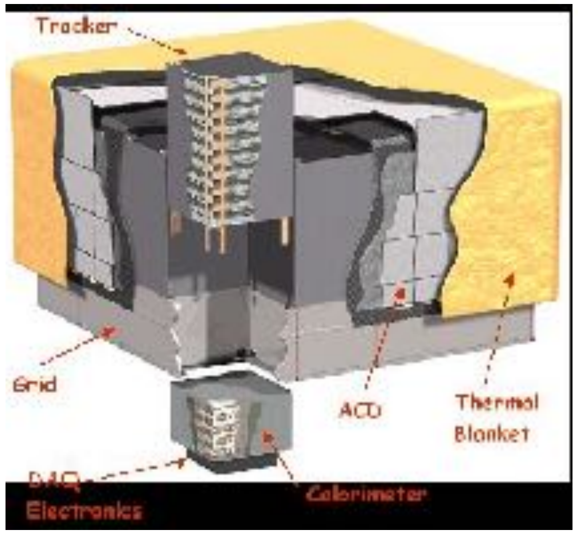

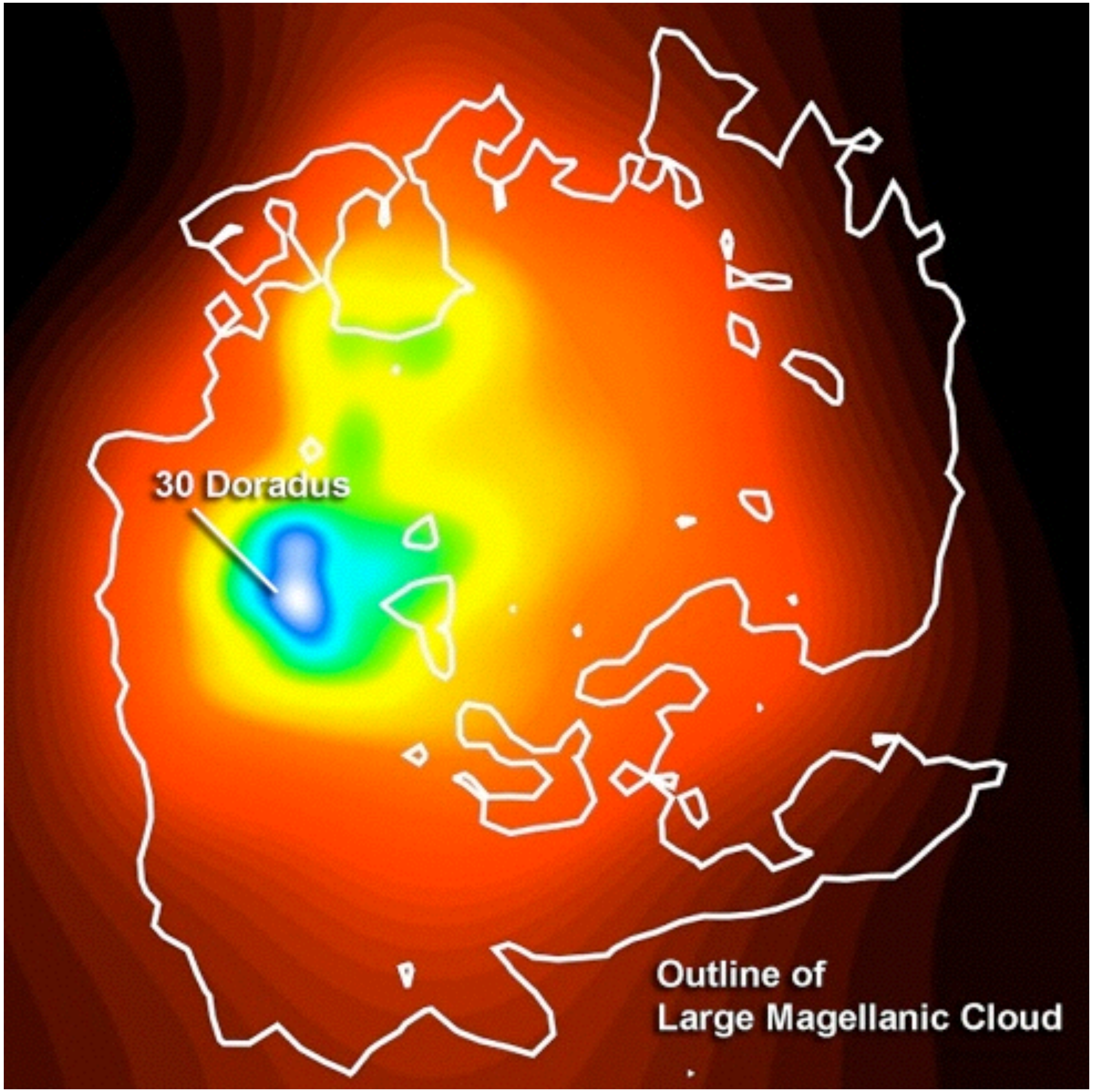

Fermi's Large Area Telescope shows that an intense star-forming region in the Large Magellanic Cloud named 30 Doradus is also a source of diffuse gamma rays. Brighter colors indicate larger numbers of detected gamma rays.

Relative importance of gamma-ray production processes

For this estimate we approximate the total proton spectrum by $N(E_p) \equiv dN/dE_p = a_p E_p^{-\alpha}$ protons GeV^{-1} cm^{-3}. For $E_\gamma \gg m_\pi c^2/2$, the γ-ray source function from π^0 production is

$$Q_{\pi^0}(E_\gamma) \approx n \left(\sigma_{pp}^{inel} \frac{2 Z_{N\pi^0}}{\alpha} \right) \times a_p \, E_\gamma^{-\alpha}, \tag{4.14}$$

where σ_{pp}^{inel} is the inelastic proton–proton cross section, n is the average matter density per cm^3 and $Z_{N\pi}$ is a spectrum-weighted moment of the momentum distribution of pions produced in proton–proton collisions [6]. The spectrum weighted moments give the yield of the process ab from a power law cosmic ray spectrum of integral spectral index γ

$$Z_{ab} \equiv \int_0^1 x_L^\gamma F(x_L) dx_L \ , \tag{4.15}$$

where x_L is the ratio of the energy of the secondary particle b to the primary energy in the Lab system. For $\alpha = 2.0$, 2.4, and 2.7 respectively, $Z_{N\pi^0} \approx$ 0.16, 0.066 and 0.035. Thus, for $\alpha = 2.7$, close to the locally measured proton spectrum

$$\boxed{Q_{\pi^0}(E_\gamma) \approx 2.5 \times 10^{-26} \, a_p \, n \, E_\gamma^{-2.7} \quad \text{photons GeV}^{-1}\ \text{s}^{-1}\ \text{cm}^{-3} \ ,} \tag{4.16}$$

from protons

where E_γ is in GeV and n is in cm^{-3}.

Relative importance of gamma-ray production processes

Similarly, we approximate the total electron spectrum by $N(E_e) \equiv dN/dE_e = a_e E_e^{-\alpha}$ electrons $\mathrm{GeV}^{-1}\,\mathrm{cm}^{-3}$. To obtain the bremsstrahlung source function, we assume that after an electron of energy E_e has traveled one radiation length, X_0, it is converted into a photon of energy $E_\gamma = E_e$. Hence,

$$Q_{\mathrm{br}}(E_\gamma) \approx N(E_\gamma) n / X_0. \tag{4.17}$$

Thus, for $\alpha = 2.7$,

$$\boxed{Q_{\mathrm{br}}(E_\gamma) \approx 1.2 \times 10^{-25} a_e n E_\gamma^{-2.7} \quad \text{photons GeV}^{-1}\,\mathrm{s}^{-1}\,\mathrm{cm}^{-3}\,.} \tag{4.18}$$

from electrons (bremsstrahlung)

Relative importance of gamma-ray production processes

For inverse Compton scattering, we approximate the photon energy after scattering by an electron of energy $E_e = \gamma m_e c^2$ by $\gamma^2 \bar{\varepsilon}$ where $\bar{\varepsilon}$ is the mean photon energy of the radiation field under consideration. Provided the Compton scattering is in the Thomson regime $(\gamma\bar{\varepsilon} \ll m_e c^2)$ this gives an inverse Compton source function

$$Q_{\rm IC}(E_\gamma) \approx N(\gamma) n_{\rm ph} \sigma_T / 2\gamma\bar{\varepsilon} \, , \tag{4.19}$$

where $N(\gamma)d\gamma = N(E_e)\, dE_e$, and we obtain

$$Q_{\rm IC}(E_\gamma) \approx a_e \frac{(\bar{\varepsilon})^{1/2}}{E_\gamma^{(\alpha-1)/2}} \frac{n_{\rm ph}\sigma_T}{m_e c^2} \, . \tag{4.20}$$

electrons inverse Compton

Relative importance of gamma-ray production processes

For scattering on the microwave background, we use $n_{\rm ph} = 400$ cm^{-3}, $\bar{\varepsilon} = 6.25 \times 10^{-4}$ eV, and obtain for $\alpha = 2.7$

$$\boxed{Q_{\rm IC}(E_\gamma) \approx 2.1 \times 10^{-24} a_e E_\gamma^{-1.85} \quad \text{photons GeV}^{-1}\ \text{s}^{-1}\ \text{cm}^{-3}\ ,} \tag{4.21}$$

where E_γ is in GeV. We note that, for an assumed matter density of 1 cm^{-3}, at 1 GeV the inverse Compton scattering contribution is an order of magnitude larger than the bremsstrahlung contribution, and the relative importance of the inverse Compton scattering contribution increases with energy. The bremsstrahlung contribution is higher than that of π^0 by about a factor of five. The π^0 γ-rays can only be important if there are many more protons than there are electrons.

from electrons (inverse Compton scattering on CMB)

More exact gamma-ray yields

previous section: estimates
main inaccuracy: energy spectra for protons and electrons are different in CRs
electrons suffer synchrotron radiation losses and have a steeper spectrum

Bertsch et al. [71] suggest the following spectrum of the galactic electrons (in $\mathrm{cm^{-2}\,s^{-1}\,sr^{-1}\,GeV^{-1}}$)

$$
\begin{aligned}
dN/dE_e &= 0.019 E_e^{-2.35} && \text{for } E_e < 5\ \mathrm{GeV} \\
&= 0.149 E_e^{-3.30} && \text{for } E_e \geq 5\ \mathrm{GeV}
\end{aligned}
\tag{4.22}
$$

INCLUSIVE (e^-+e^+) spectrum below 1 TeV (AMS-02, FERMI & PAMELA)

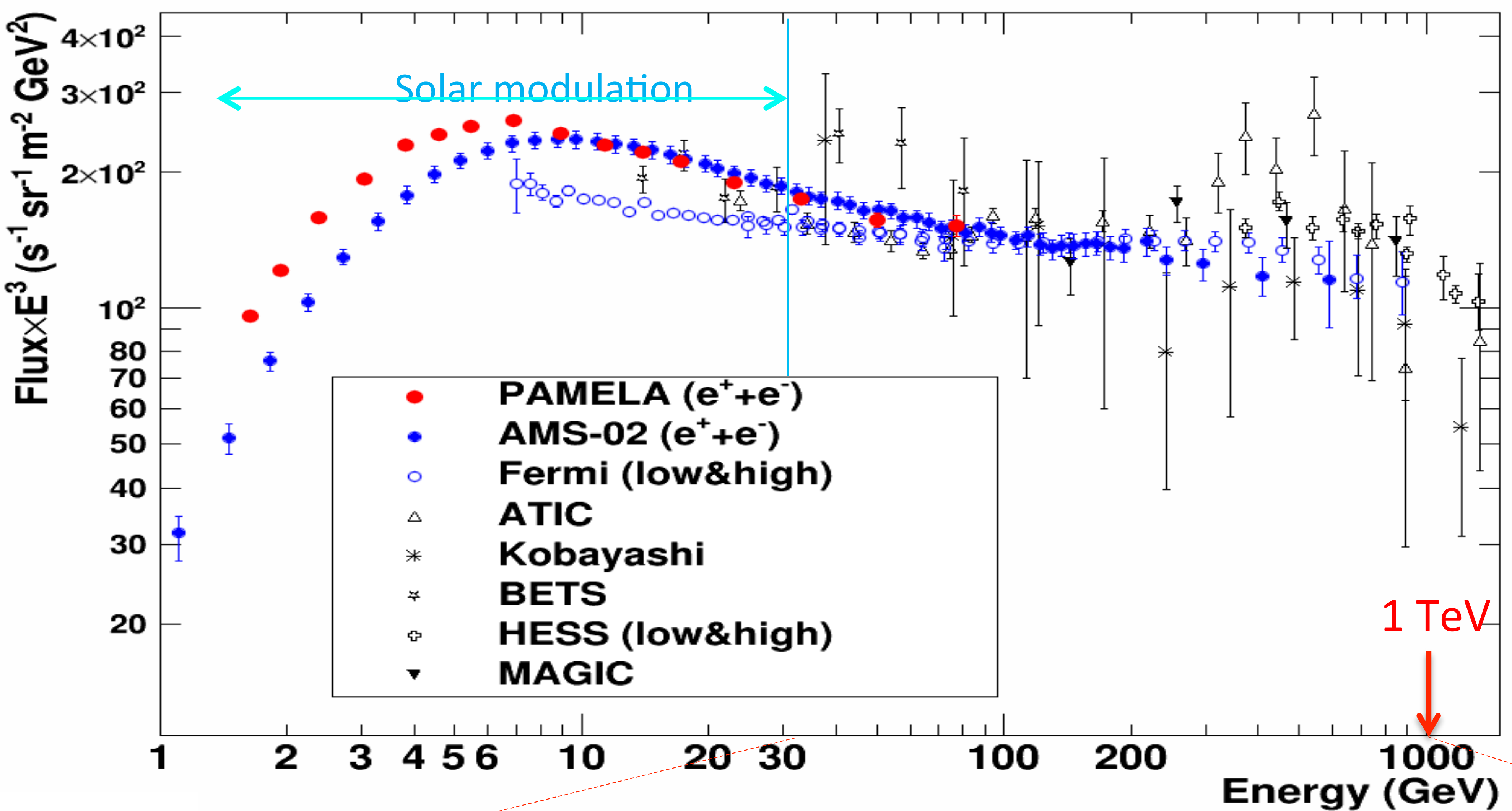

Figure 4.8 shows the source functions of the three processes using the electron spectrum given by (4.23) and a proton spectrum $dN/dE_p = 3.06E_p^{-2.70}$. The matter density for π^0 and bremsstrahlung is 1 (atom/cm^3) and the microwave background is used as target for the inverse Compton effect. The π^0 yield peaks at $E_\gamma = m_{\pi^0}/2 \simeq 70$ MeV but in Fig. 4.8 the peak appears at higher energy because it is shifted by the E_γ factor. The bremsstrahlung spectrum dominates at lower energies and clearly follows the break in the electron spectrum. The inverse Compton spectrum is indeed very flat ($\sim E_\gamma^{(\alpha+1)/2}$) and approaches the π^0 contribution at $E_\gamma = 10^4$ GeV in spite of the much steeper electron spectrum.

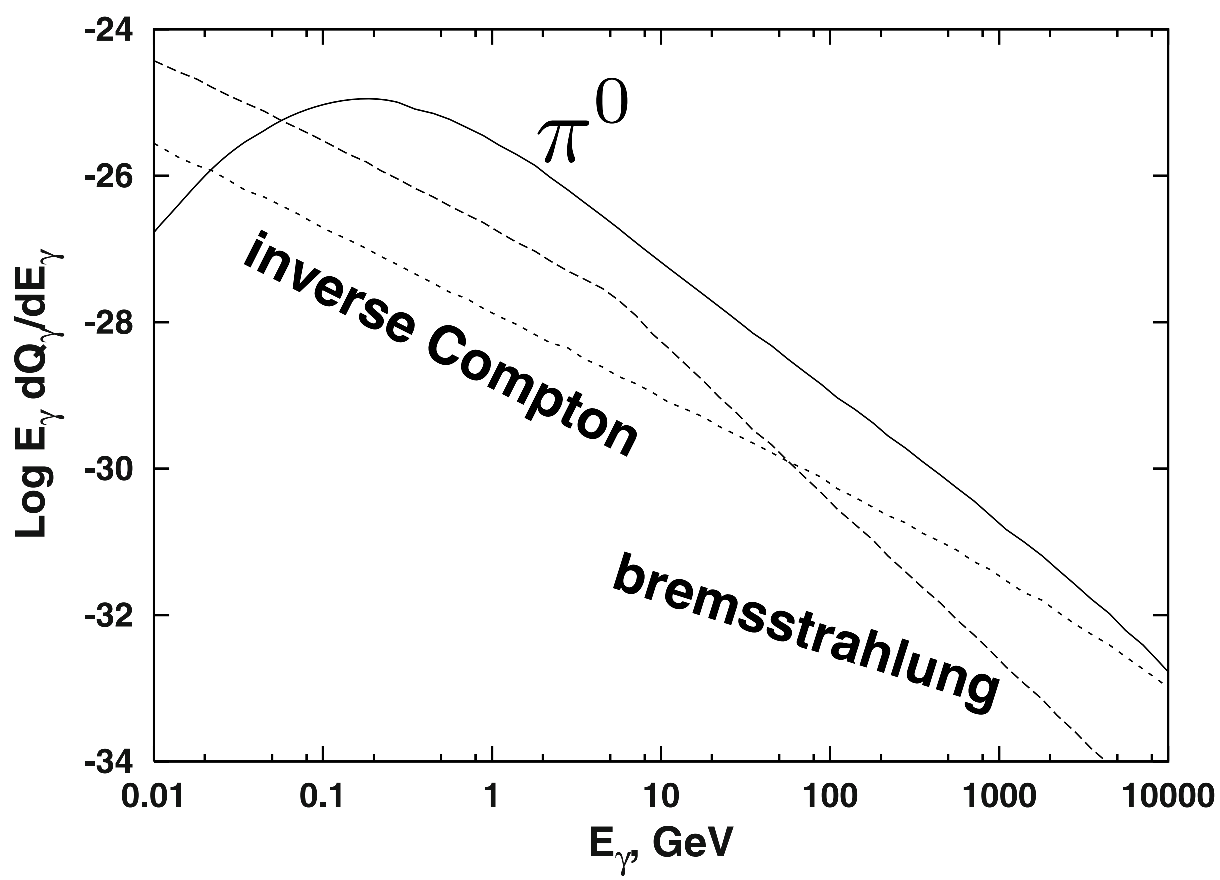

More exact gamma-ray yields as obtained with MC calculations

Fig. 4.8. Yields of the γ-ray production by π^0 (solid line), bremsstrahlung (dashes) and inverse Compton (dots) for the proton and electron spectra described in the text.

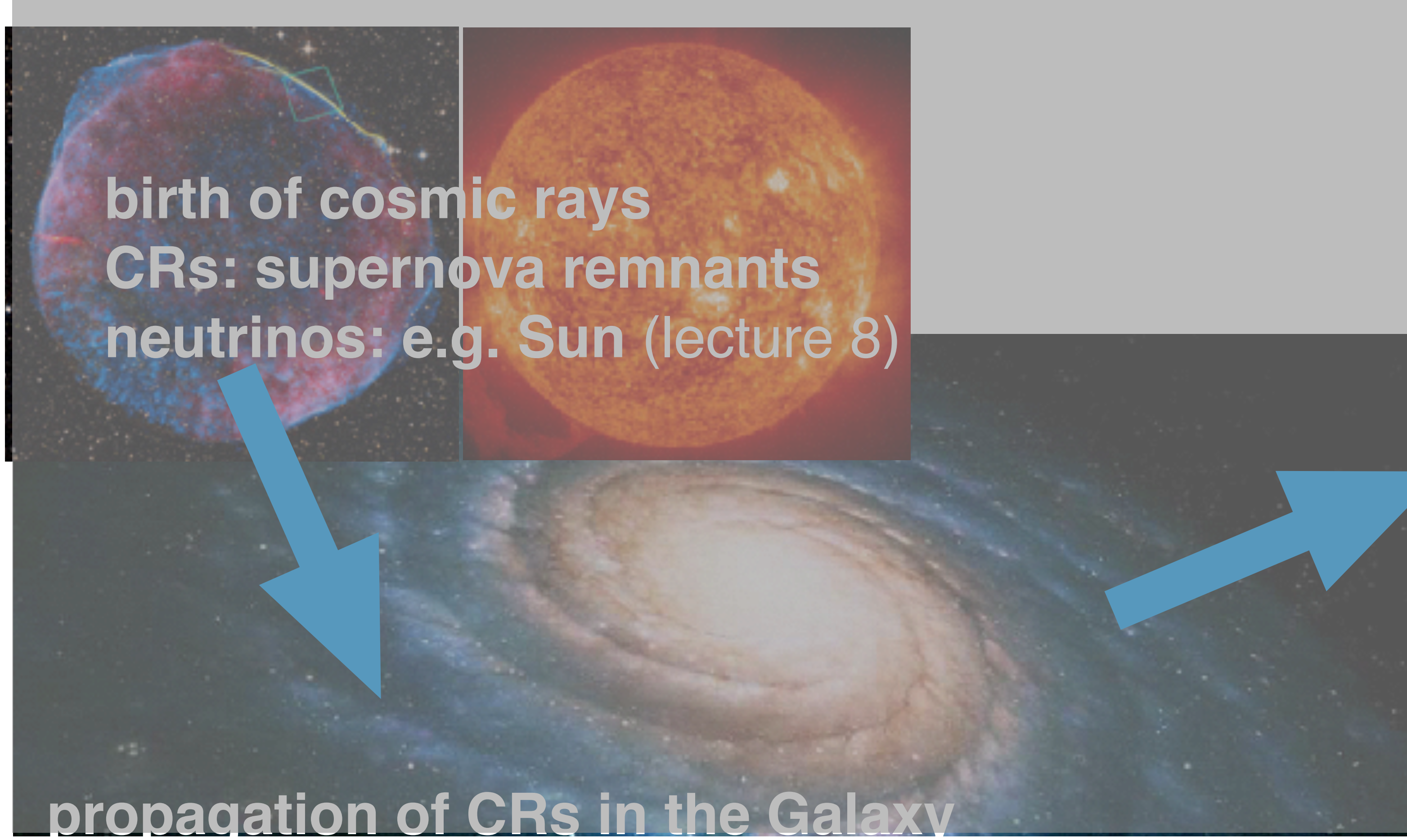

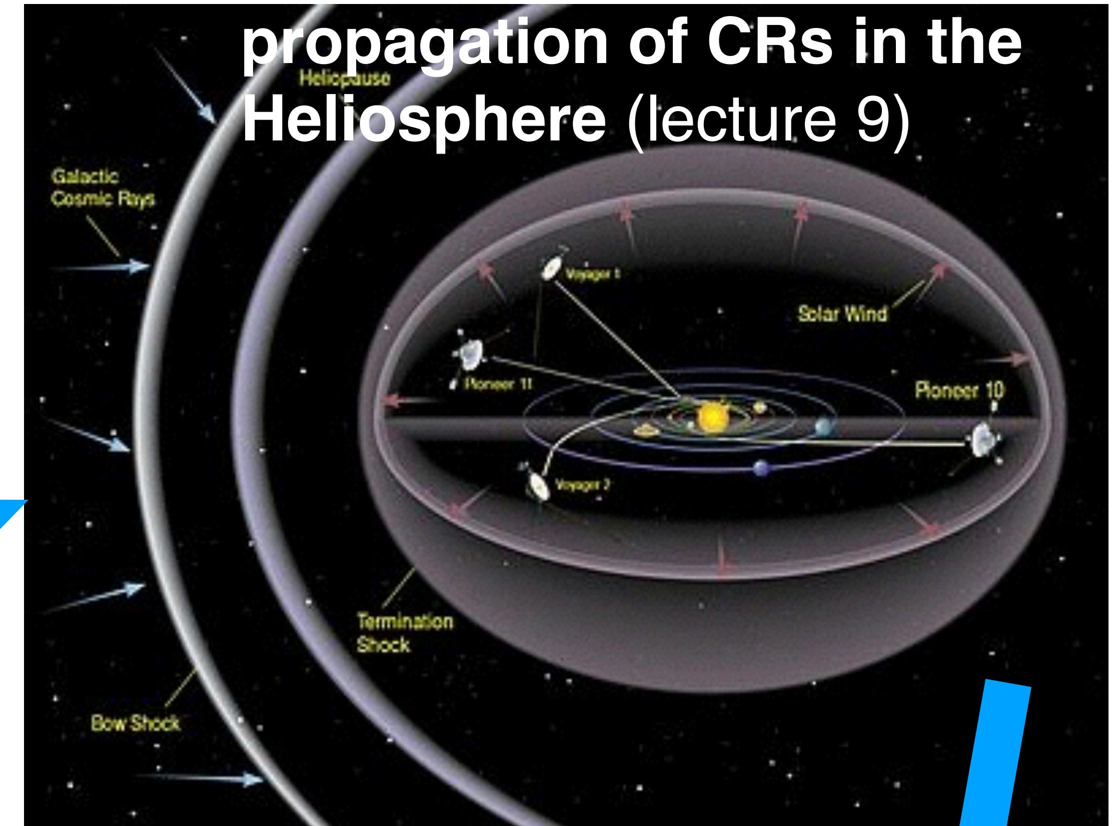

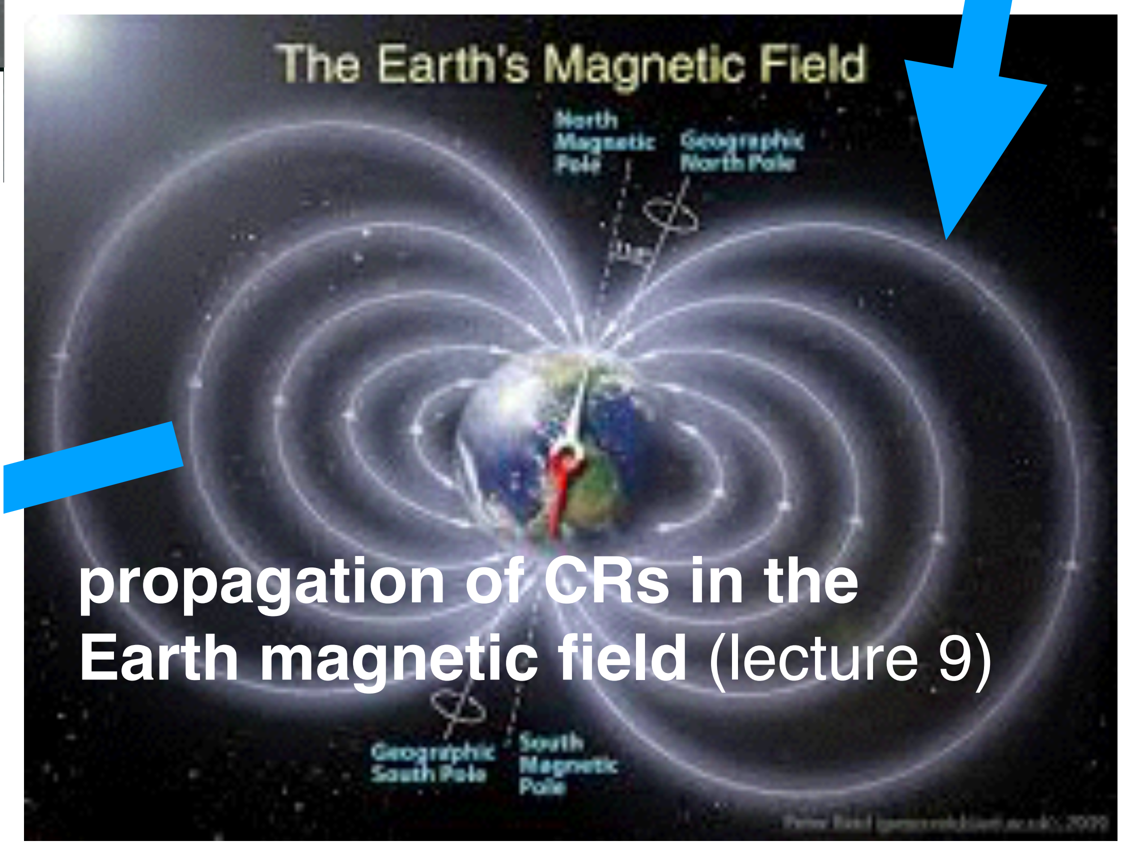

today:
Stanev, chapter 5

1+12)

Cosmic rays at the top of the atmosphere

Stanev chapter 5

galactic cosmic rays are influenced by
- solar magnetic field/heliosphere
- Earth magnetic field

cosmic rays interact in the atmosphere of the Earth
—> measurements above the atmosphere with balloons and satellites

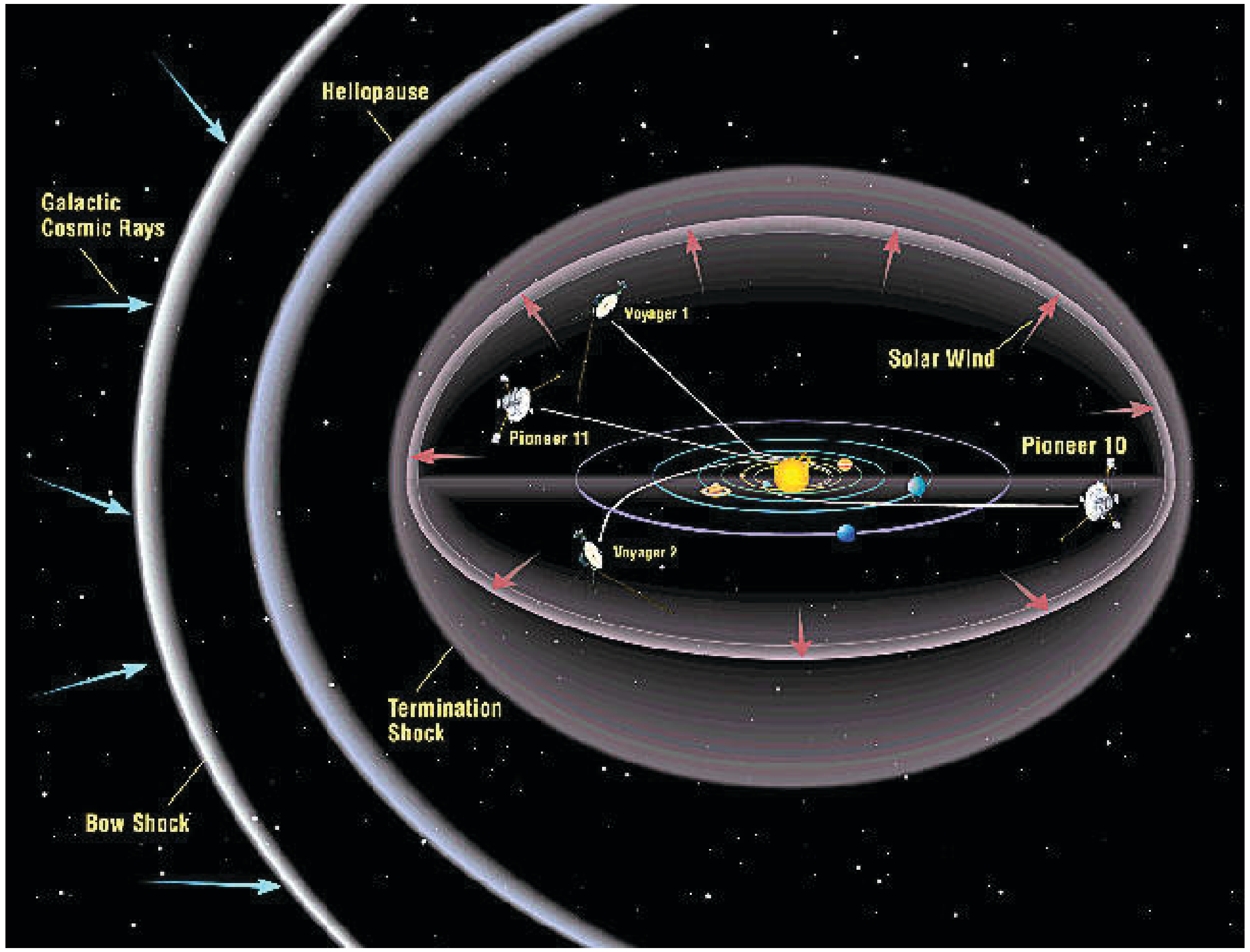

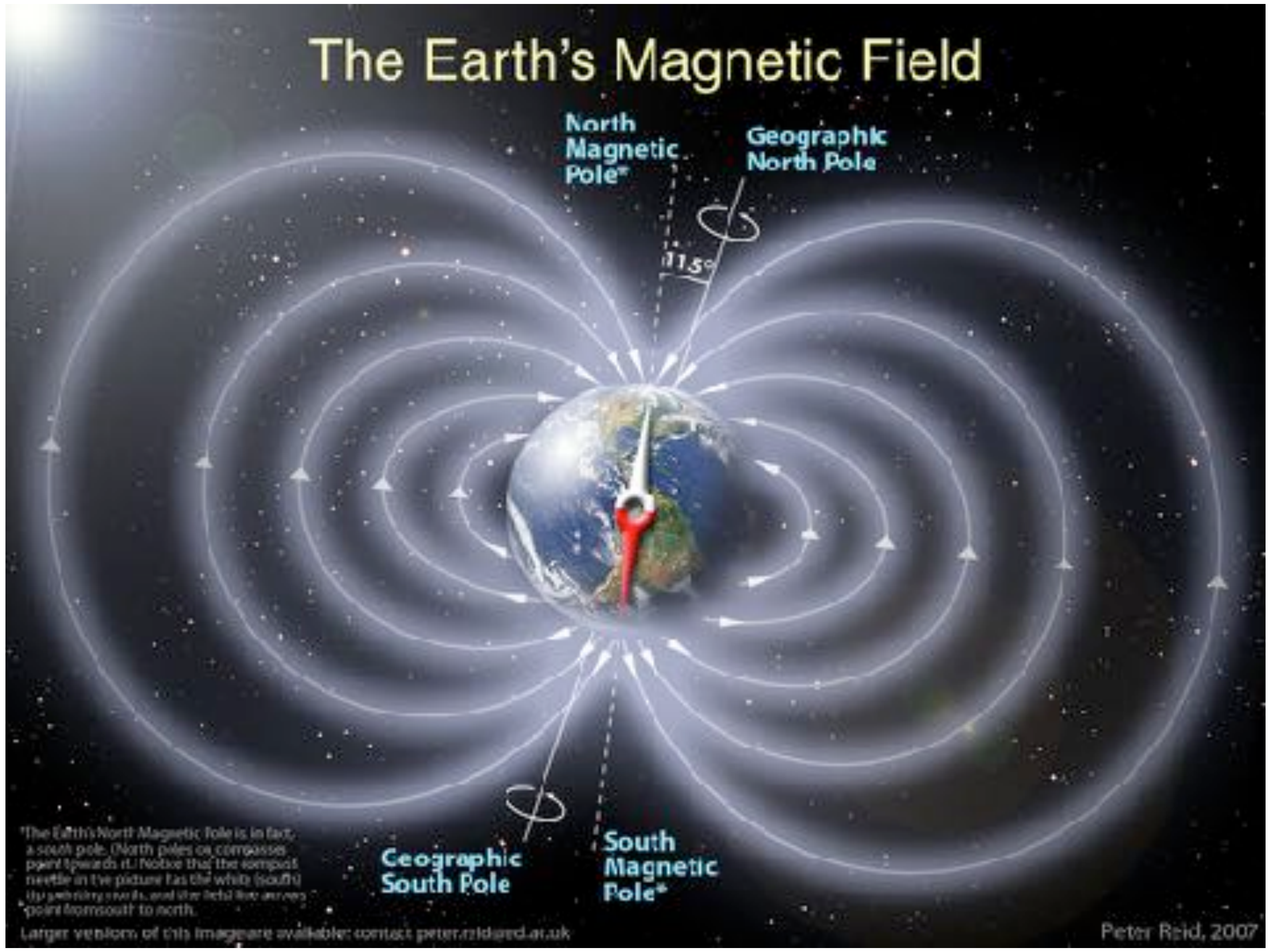

Solar modulation

outflow material from surface of Sun —> solar wind
B field frozen in and carried by solar wind

The solar wind originates in the solar corona which has a temperature of about 10^6 K, a factor of hundred higher than the photosphere of the Sun. The magnetic field is frozen in the ionized material and is dragged outwards from the Sun. The field is attached to the rotating Sun and the expansion leads to the creation of an Archimedes spiral which is the large-scale field structure. This structure was named the *Parker spiral*. The radial and azimuthal components of the magnetic fields are

$$\boxed{B_r = B_\odot R_\odot^2 \frac{1}{r^2}} \quad \boxed{B_\phi = B_\odot R_\odot \frac{\sin\theta}{r}} , \qquad (5.1)$$

where $B_\odot$ is the magnetic field on the surface of the Sun, $R_\odot$ is the solar radius and θ is the zenith angle measured from the center of the Sun. At sufficiently large distance from the Sun the radial component vanishes and the azimuthal component, which can be approximated as circular, dominates.

Parker Spiral

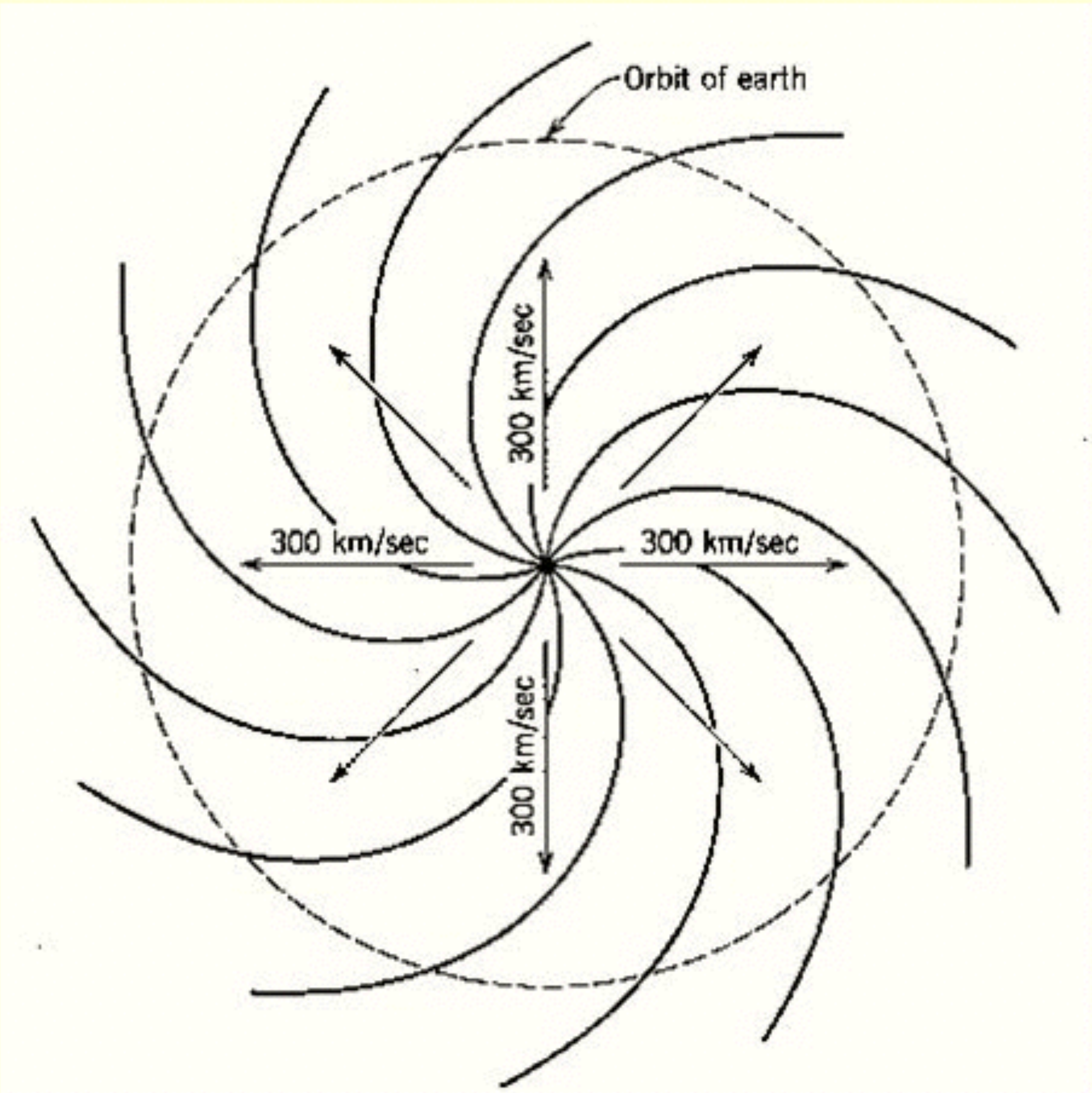

- The solar wind flows radially outward at ~ 400 km/s
- Solar rotation period at equator ~25 days
- Results in Parker Spiral
- Left is view looking down on ecliptic
- Magnetic field ~ 45 degrees to Earth-Sun line at 1AU

Solar modulation

The solar wind carries along the magnetic fields characteristic for the hot coronal regions. In the vicinity of Earth the solar wind particles, mostly protons, have velocities of 300 to 600 km/s, which corresponds to an average kinetic energy of 500 eV. The solar wind flux is 1.2×10^8 cm^{-2} s^{-1} and its energy density is about 2.5 KeV cm^{-3}. The magnetic field strength is about 5×10^{-5} G which translates into energy density 40 times lower than that of the solar wind particles.

Proceedings of ICRC 2001: 3769 © Copernicus Gesellschaft 2001

ICRC 2001

Solar Modulation of Cosmic Rays

Solar modulation of the galactic cosmic ray spectra since the Maunder minimum

G. Bonino[1], G. Cini Castagnoli[1], D. Cane[1], C. Taricco[1], and N. Bhandari[2]

[1]Dipartimento di Fisica Generale, Universit di Torino and Istituto di Cosmogeofisica, CNR, To rino, Italy
[2]Physical Research Laboratory, Ahmedabad, India

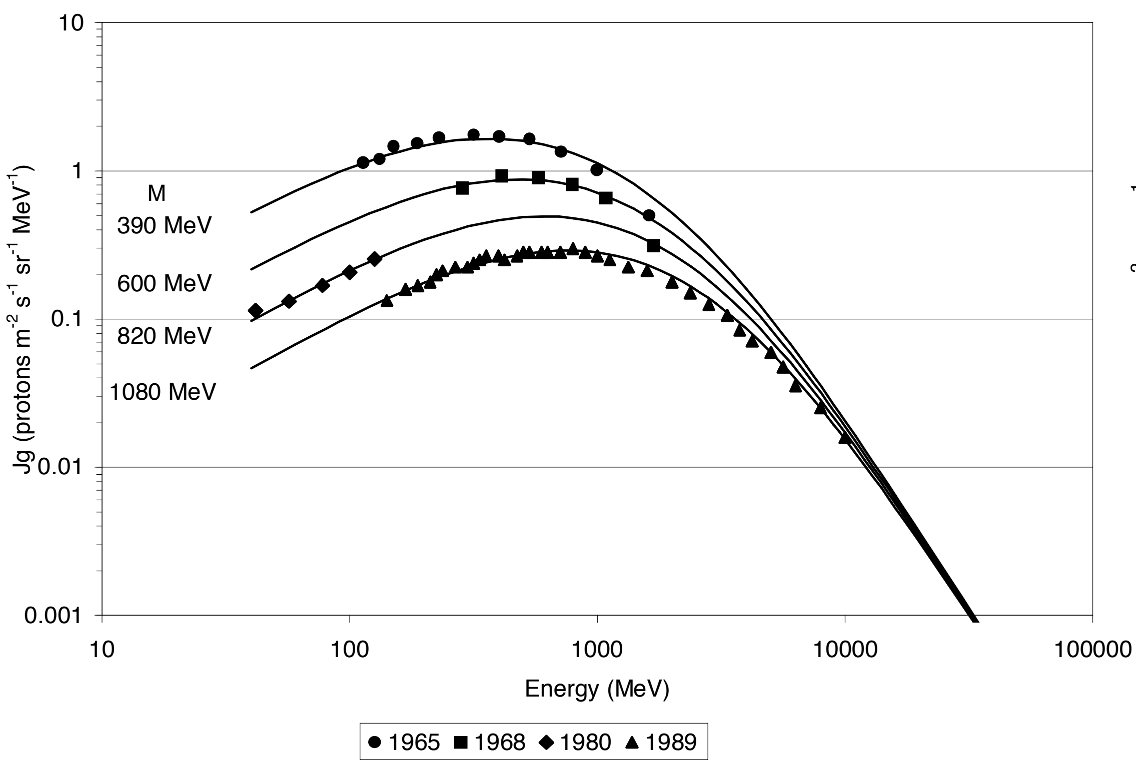

Fig. 1. Differential cosmic-ray spectra obtained from Eq. (1) for different values of the solar modulation parameter M = 390, 600, 820, 1080 MeV corresponding to the measurements performed with balloons or spacecrafts during 1965, 1968, 1980 and 1989 respectively.

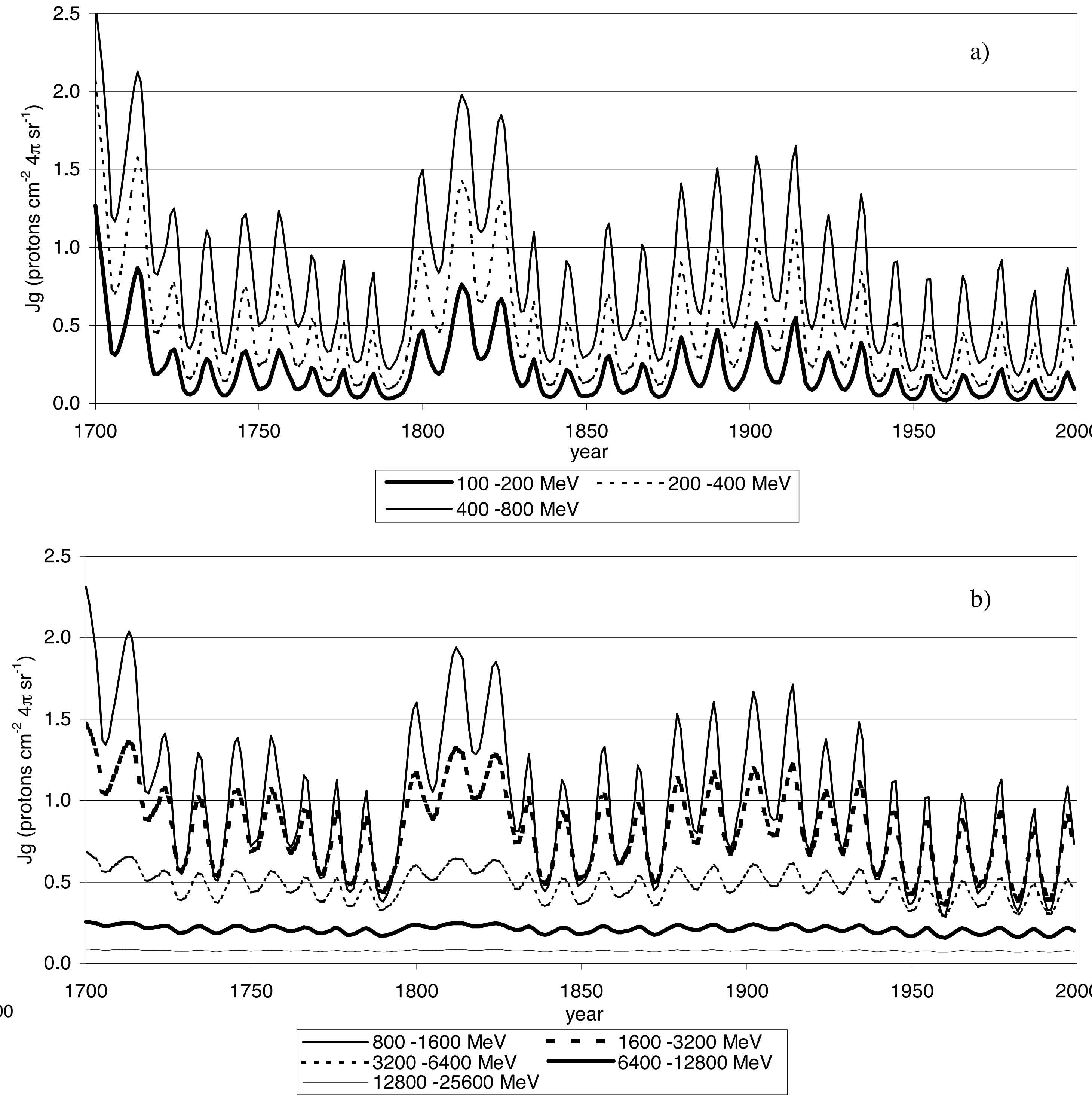

Fig. 2. Proton flux $J_G(t)$: a) for the kinetic energy intervals ΔT = 100-200 MeV, 200-400 MeV, 400-800 MeV; b) for ΔT = 800-1600 MeV, 1600-3200 MeV, 3200-6400 MeV, 6400-12800 MeV, 12800-25600 MeV.

Solar modulation

standard three-dimensional spherically symmetric model of solar modulation

- cosmic ray diffusion through the magnetic field carried by the solar wind,
- the convection by the outward motion of the solar wind, and
- the adiabatic deceleration of the cosmic rays in this flow.

The first two processes lead to a rigidity dependent decrease of the particle flux. The third one leads to a decrease of the energy of the particles that penetrate the heliosphere.

LEAP has normalized the cosmic ray spectra of protons and helium to their measured high energy shape. At rigidities exceeding 20 GV cosmic rays are not affected by the solar wind. The diffusion coefficient used $\kappa = C_0 \beta R$ is proportional to the particle rigidity where the coefficient C_0 is adjusted to match the detected flux at high energy. The solar wind speed v is taken to be 400 km/s. The data is best fit by a solar modulation parameter $\phi = 500 \pm 75$ MV. The solar modulation parameter is the integral

$$\boxed{\phi = \frac{1}{3} \int_{r_1}^{r_{hs}} \frac{v}{\kappa}\, dr,} \tag{5.2}$$

where r_1 is the heliospheric radius of the Earth (1 AU) and r_{hs} is the boundary of the heliosphere assumed here to be 50 AU. Current data suggest that the boundary is further away, not any closer than 80 AU.

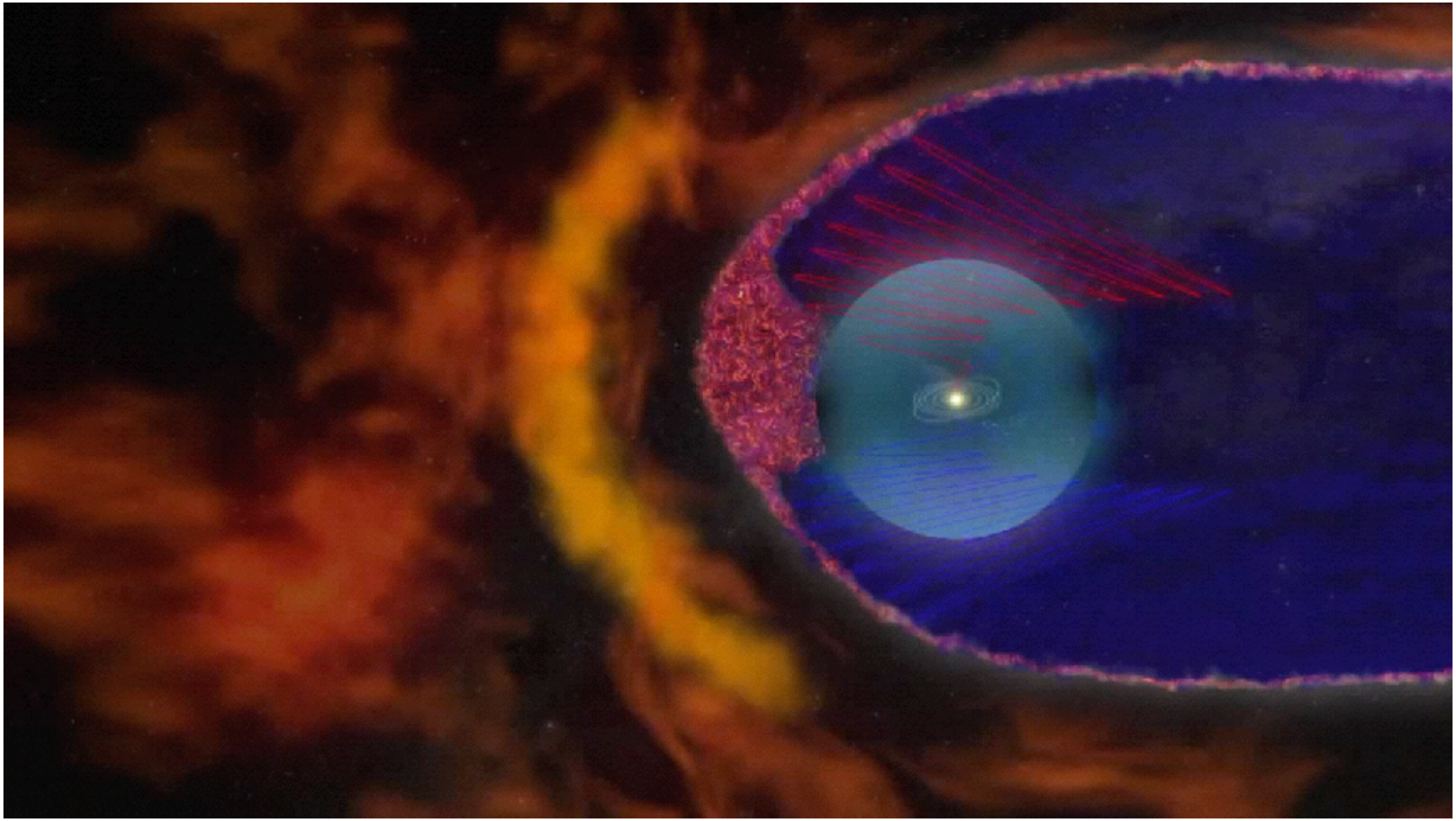

This animation depicts the effect of the new scenario on galactic cosmic rays. The heliospheric boundaries are very important in shielding the inner solar system from the galactic cosmic ray flux. The heliopause, the last region that separates us from the rest of the galaxy, acts more like a membrane that is permeable to galactic cosmic rays than a shield that deflects those energetic particles. The galactic cosmic rays slowly wander into the heliosphere and can get trapped in the sea of magnetic bubbles. Eventually they access the solar magnetic field lines that connect back to the sun, and can move quickly towards the sun and Earth.

Solar modulation

In the force field approximation [107] the effect of solar modulation is expressed in terms of the single modulation parameter ϕ. A particle that has total energy E_{IS} in interstellar space would reach the Earth with energy $E = E_{IS} - |Z|\phi$, where Z is its charge. The flux of particles of that type at Earth Φ is related to the interstellar flux Φ_{IS} as

$$\boxed{\Phi(E) = \frac{(E^2 - m^2)}{(E_{IS}^2 - m^2)} \times \Phi_{IS}(E_{IS}) \, ,} \tag{5.3}$$

where m is the particle mass. The first term in (5.3) accounts for the loss of flux and the second one accounts for the particle energy loss.

Solar modulation

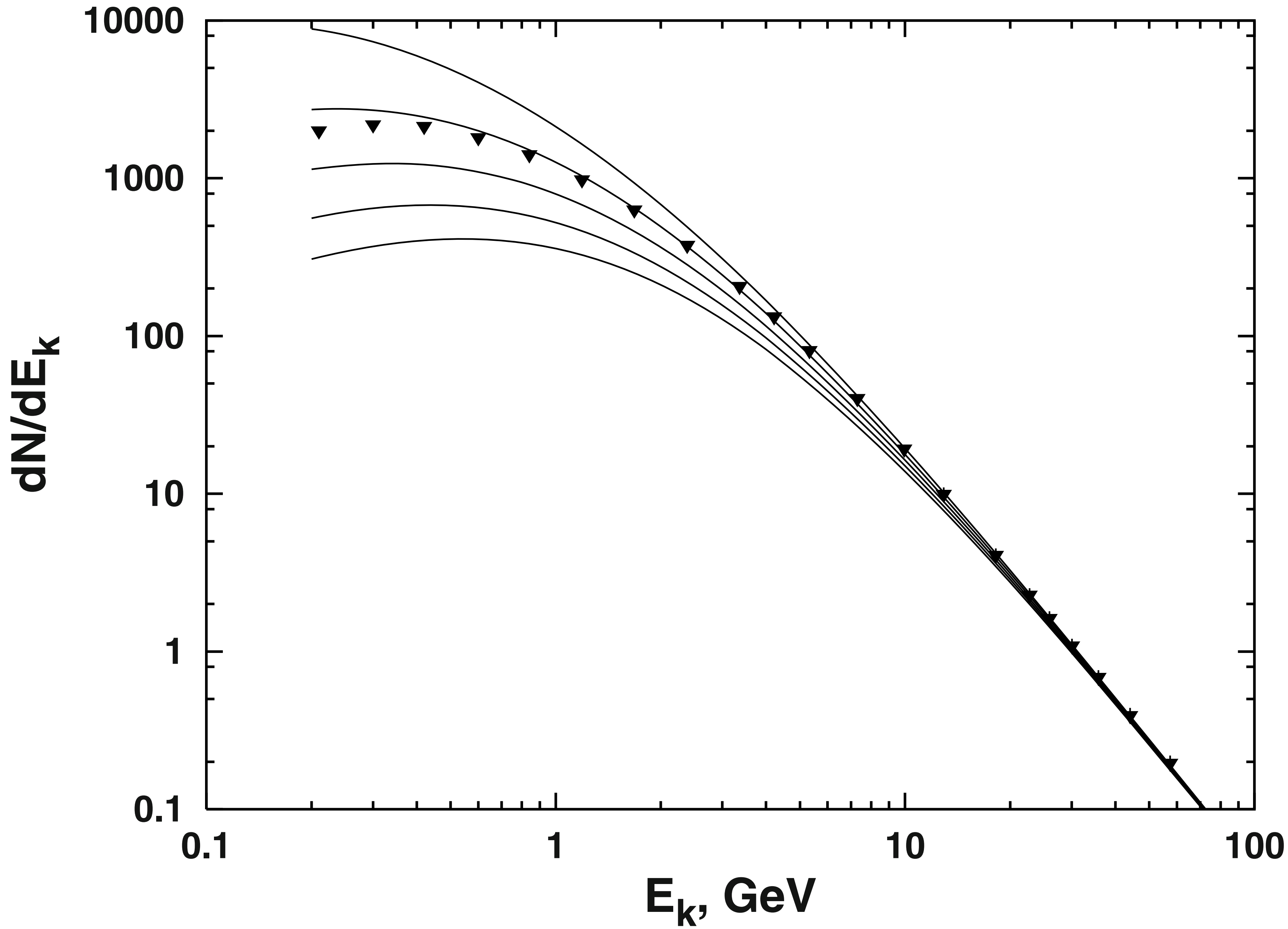

Fig. 5.6. Comparison of the LEAP proton flux to a fit of the measurements above 20 GeV with solar modulation using modulation parameters $\phi = 200, 400, 600, 800,$ and 1,000 MV from top to bottom. The modulation is performed under the force field approximation (5.3).

Galactic Cosmic Rays and the Heliosphere

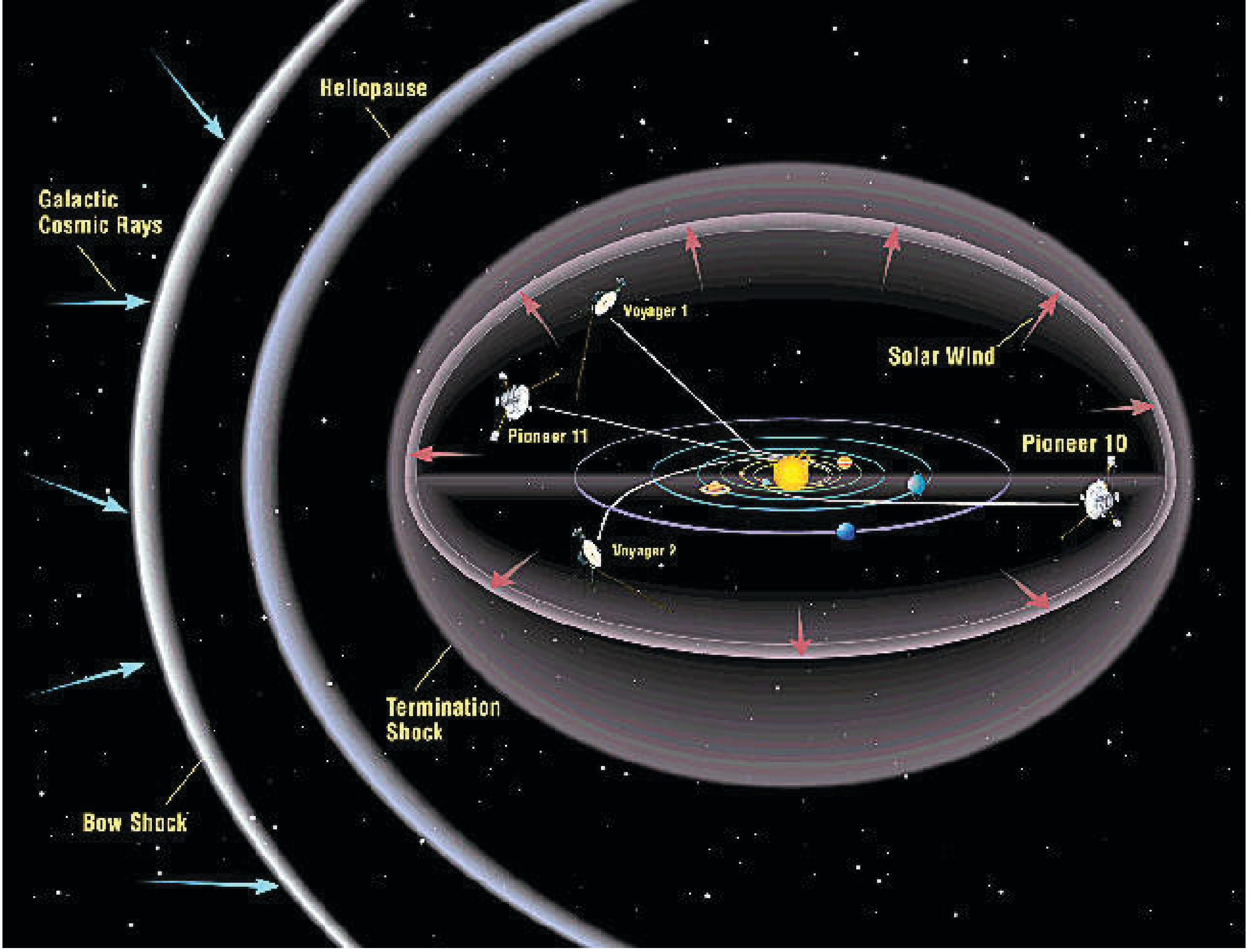

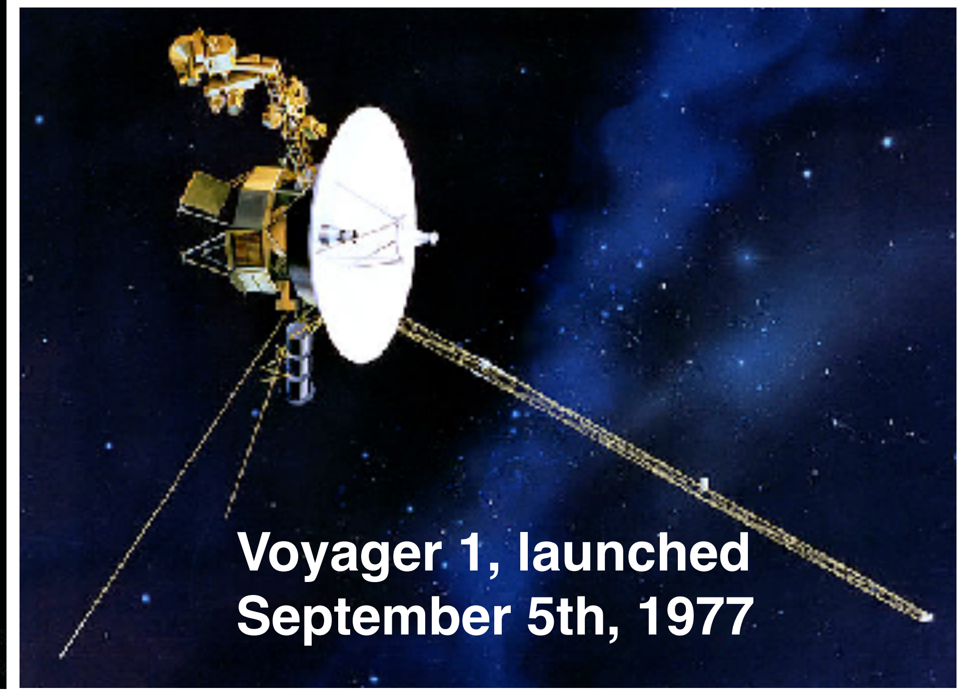

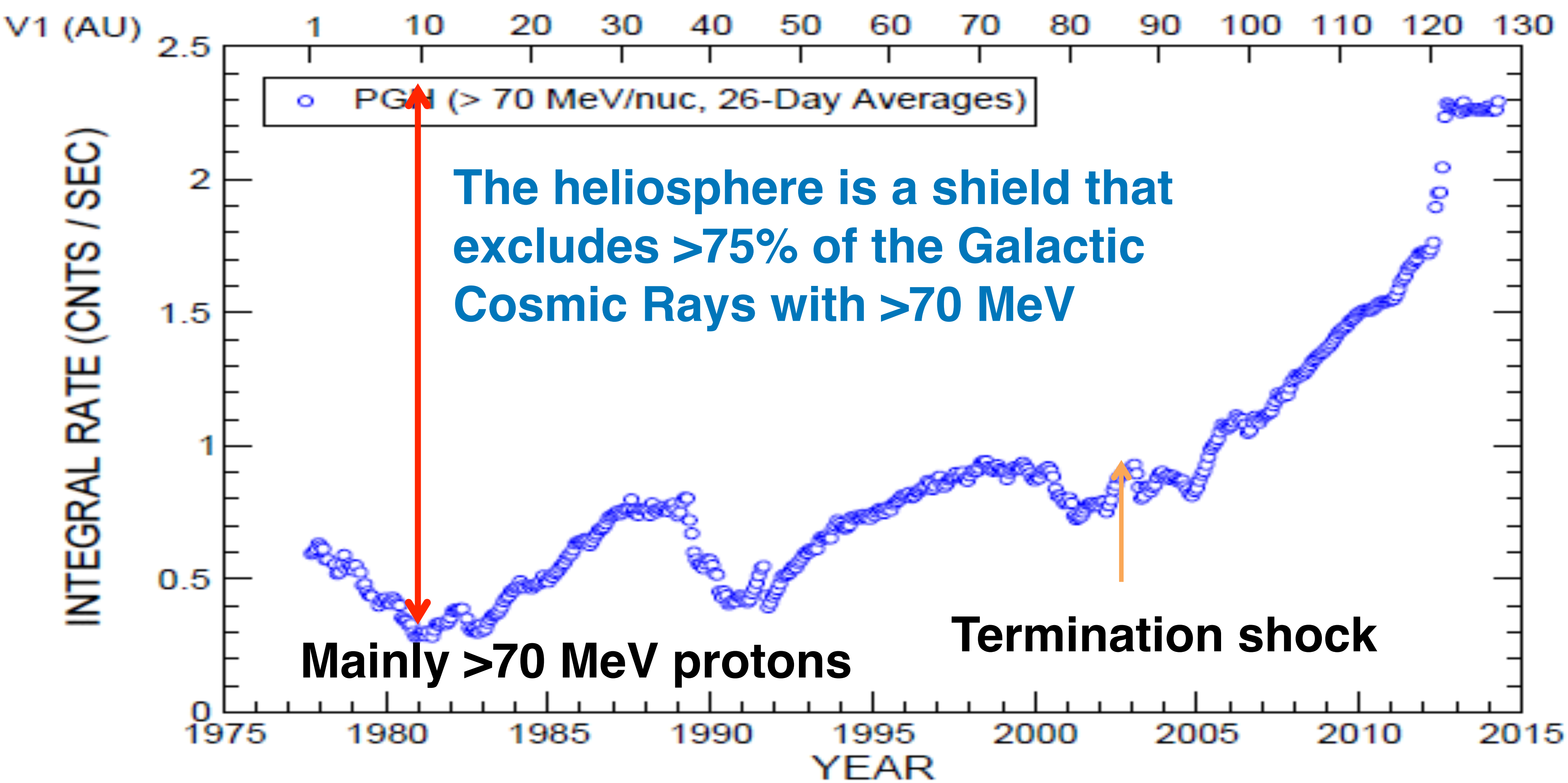

Geomagnetic field effects

geomagnetic field bends trajectories of charged particles

The cosmic ray flux on top of the atmosphere is therefore not isotropic and depends on the detector position $\boldsymbol{x}$, $\Phi(R,\ \boldsymbol{x}_d,\ \Omega) = \Phi_0(R) \times \epsilon_B(r,\ \boldsymbol{x}_d,\ \Omega)$, where $\Phi_0(r)$ is the flux at distances more than several earth radii, already corrected for the solar modulation. The penetration probability, ϵ_B, can take only the discrete values 0 or 1, i.e. a particle can or cannot reach the position $\boldsymbol{x}$ as a function of its rigidity R and the angle of its motion in the geomagnetic field frame.

Geomagnetic field effects

Stoermer [109] had solved analytically the equation of motion for the case of a dipole field and neglecting the shadow of the Earth even before the discovery of cosmic rays. The solution expresses the particle motion in units of Stoermer radius $r_S = \sqrt{(\mu_0 M/4\pi R)}$, where M is the magnetic dipole moment of the Earth ($M \simeq 8.1 \times 10^{25}$ G cm^3). For particles that penetrate vertically towards the center of the magnetic dipole the minimum rigidity required for penetrating to distance r from the center of the magnetic dipole is

$$\boxed{R_S \geq 59.4\,\mathrm{GV} \times \left(\frac{r_\oplus}{r}\right) \cos^4 \lambda_B/4\,,} \tag{5.4}$$

where λ_B is the magnetic latitude and 59.4 GV $\simeq M/(2r_\oplus^2)$ is the rigidity of a particle in a circular orbit of radius $r_\oplus$ in the equatorial plane of the dipole field. The minimum rigidity for a particle that penetrates to the surface of the Earth at the magnetic equator is correspondingly ~14.9 GV (total energy of 14.9 GeV for protons or about 7.5 GeV/nucleon for He nuclei). At magnetic latitude of ±60° the minimum rigidity is 0.93 GV which translates to energies of 1.32 and 1.05 GeV/nucleon. The vertical cutoffs change slightly with altitude throughout the atmosphere.

1931-34 A.H. Compton 12 expeditions → ~100 locations

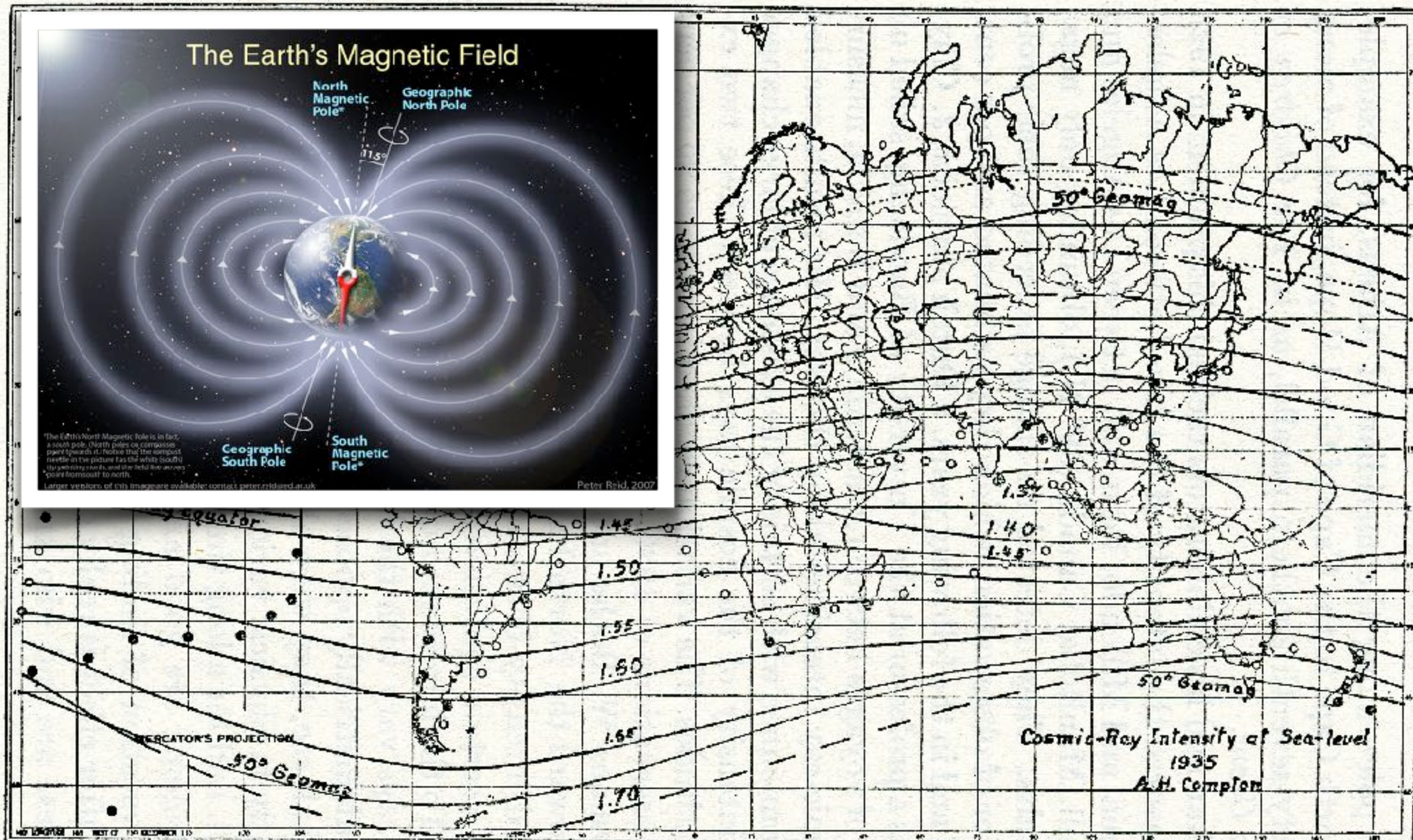

FIG. 6.—Compton's world map of isocosms. Note the parallelism of these lines of equal cosmic-ray intensity and the dotted curves of geomagnetic latitude (50° N. and S.).

→ **cosmic rays are charged particles**

Geomagnetic field effects

The complete formula for the Stoermer rigidity cutoff, R_S, is

$$\boxed{R_S(r, \lambda_B, \theta, \varphi_B) = \left(\frac{M}{2r^2}\right) \left\{ \frac{\cos^4 \lambda_B}{[1 + (1 - \cos^3 \lambda_B \, \sin\theta \, \sin\varphi_B)^{1/2}]^2} \right\}}, \quad (5.5)$$

where θ is the particle zenith angle and φ_B is the azimuthal angle measured clockwise from the direction of the magnetic south. The dependence on φ_B contains the well known east–west effect: for positively charged particles at the same zenith angle the cutoff is higher from the east direction and vice versa for negatively charged particles. The expression $\cos^3 \lambda_B \sin\theta \sin\varphi_B$ has a maximum for $\sin\varphi_B = -1$, pointing roughly at the geographical East direction, 270° clockwise from the geographic south.

~1937 East-West Effect of Cosmic-Ray Intensity

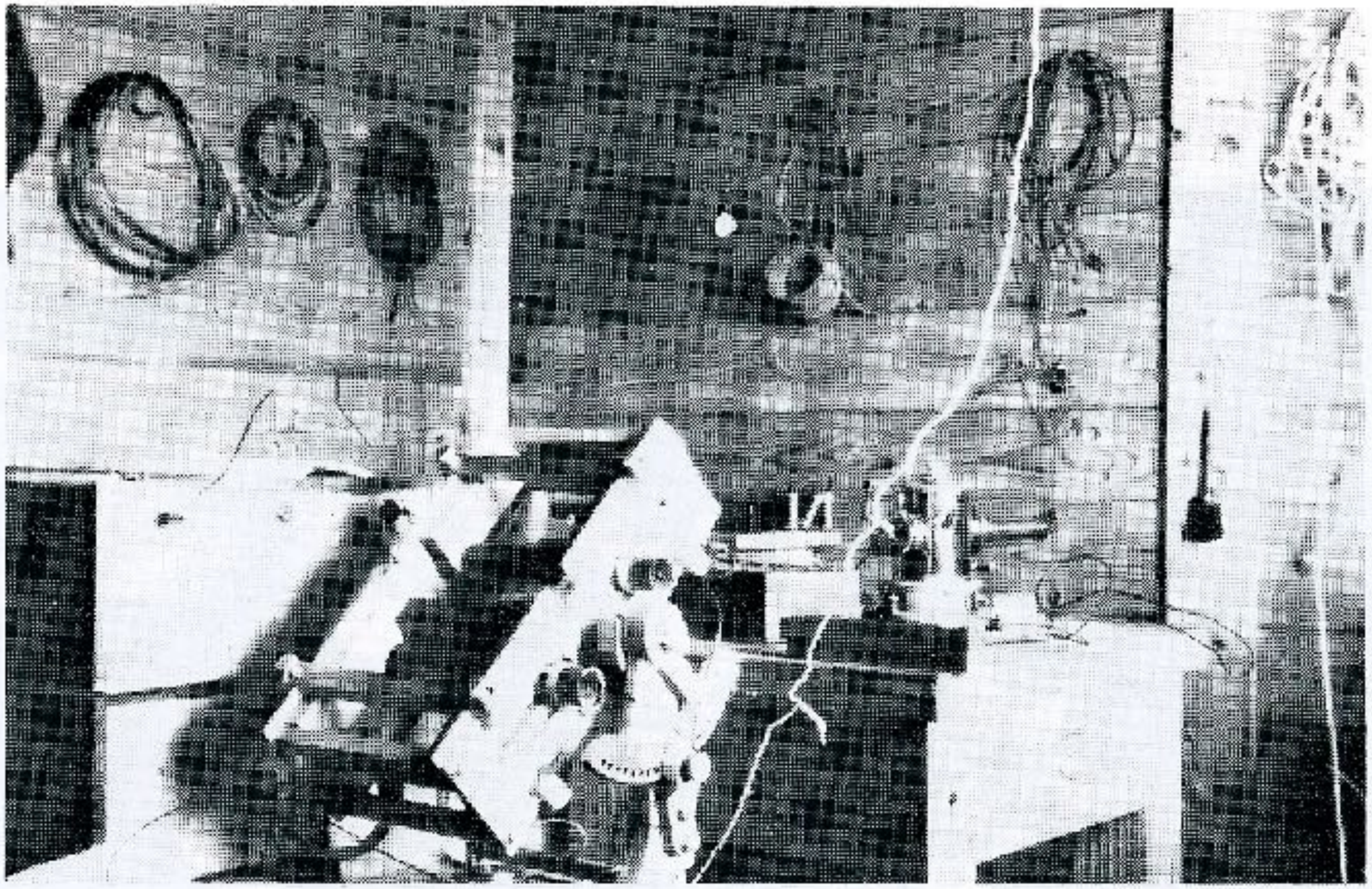

Fig. 14. The equipment for the E-W experiment.

Rossi and others

higher intensity from the west

→ cosmic rays are mostly positively charged

Daily and annual modulations

The magnetic field in the vicinity of the Earth has also a contribution from electric currents in the solar system. This part of the field introduces a time dependence of the geomagnetic cutoffs. Periodicities of 1 year and 24 hours are present, as well as more complex time variations related to the level of solar activity. These variations of the 'external' magnetic field can additionally modify the cutoffs and have to be taken into account for short-duration experiments.

small effects (on the level < ~1%)
for CRs with low energies

Daily and annual modulations

29th International Cosmic Ray Conference Pune (2005) **2**, 135–138

Solar modulation of cosmic rays in the energy range from 10 to 20 GeV

I. Braun[a,1], J. Engler[a], J.R. Hörandel[a] and J. Milke[a]

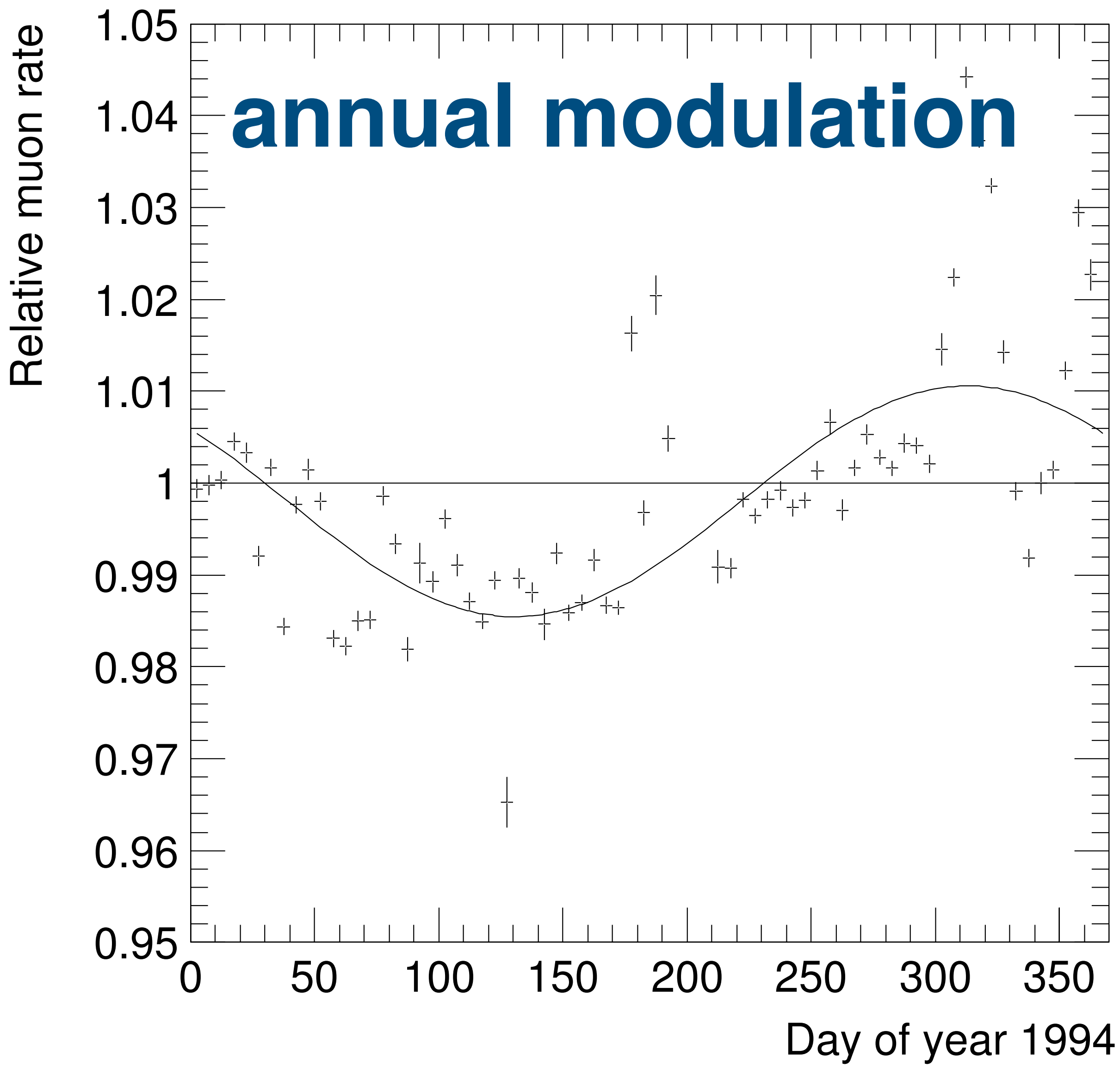

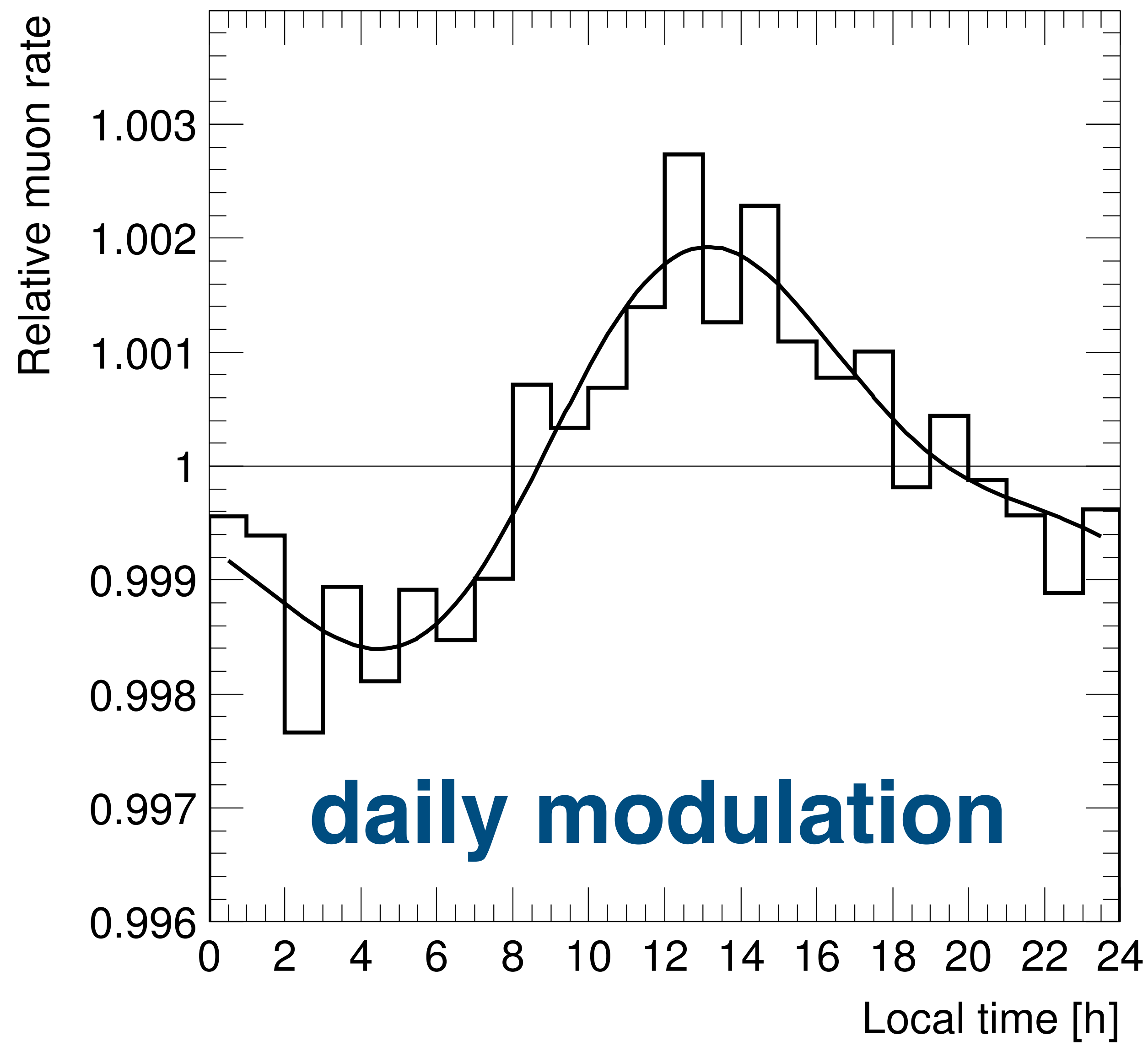

Figure 3. *Left:* Average diurnal variation of the muon rate after atmospheric correction and normalization to the daily average.

Figure 2. *Left:* Measured annual variation of the muon rate in 1994.